ANALYSIS OF C60 AND MXENE NANOCOMPOSITE BASED ELECTRODE MATERIALS FOR ENERGY STORAGE DEVICES

Author

HASSAN BUKHARI

00000275970

MS-18 (EE)

Supervisor

DR. SAIFULLAH AWAN

DEPARTMENT OF ELECTRICAL ENGINEERING

COLLEGE OF ELECTRICAL AND MECHANICAL ENGINEERING

NATIONAL UNIVERSITY OF SCIENCES AND TECHNOLOGY

ISLAMABAD

AUGUST, 2022

ANALYSIS OF C60 AND MXENE NANO-COMPOSITE BASED ELECTRODE MATERIALS FOR ENERGY STORAGE DEVICES

Author

HASSAN BUKHARI

00000275970

A thesis submitted in partial fulfilment of the requirements for the degree of MS Electrical Engineering

Thesis Supervisor:

DR. SAIFULLAH AWAN

Thesis Supervisor's Signature: _____

DEPARTMENT OF ELECTRICAL ENGINEERING
COLLEGE OF ELECTRICAL AND MECHANICAL ENGINEERING
NATIONAL UNIVERSITY OF SCIENCES AND TECHNOLOGY
ISLAMABAD

AUGUST, 2022

Declaration

I certify that this research work, titled *"ANALYSIS OF C60 AND MXENE NANO-COMPOSITE BASED ELECTRODE MATERIALS FOR ENERGY STORAGE DEVICES"* is my own work. This work is not presented elsewhere for assessment. The material used from other sources are properly acknowledged/referred.

_____

Signature of Student

HASSAN BUKHARI

NUST2018EME00000275970

Plagiarism Certificate (Turnitin Report)

This thesis has been Checked for Plagiarism. Turnitin report endorsed by Supervisor is attached.

Signature of Student

HASSAN BUKHARI

NUST2018EME00000275970

Signature of Supervisor

DR. SAIFULLAH AWAN

Language Correctness Certificate

This thesis has been read by an English expert and is free of typing, syntax, semantic, grammatical and spelling mistakes. The thesis is also according to the format given by the university.

_____

Signature of Student

HASSAN BUKHARI

NUST2018EME00000275970

_____

Signature of Supervisor

DR. SAIFULLAH AWAN

COPYRIGHT STATEMENT

Acknowledgements

I am thankful to my Creator Allah Subhana-Watala to have guided me throughout this work at every step and for every new thought which Alllah setup in my mind to improve it. Indeed, I could have done nothing without Allah's priceless help and guidance. I would also like to express special thanks to my supervisor Dr. Saif Ullah Awan for his help throughout my thesis and also for (EE 805) Semiconductor Processing and (EE 806) Thin Film processing courses which he has taught me. I can safely say that I haven't learned any other engineering subject in such depth than the ones which he has taught. I would also like to pay special thanks to Ms. Sana Zainab and Sr. Dr. Saifullah Awan for their tremendous support and cooperation. Each time I got stuck in something, both came up with the solution. I would also like to thank Sr. Dr. Syed Rizwan (Co-Supervisor),and Ms. Afsheen (PhD Scholar) for being on my thesis guidance and evaluation committee. I am also thankful to Mr. Saad Saud (MS Scholar) for his support and cooperation. I am thankful to my friends and class fellows and whole team of LAB-103 in SNS block NUST for their support. Last but not least I am also thankful to my GEC Members Brig. Dr. Mashood Ahmad and Brig. Dr. Tahir Zaidi for their precious guidance and valuable feedback during research phase. I am also Thankful to Staff of EME College for providing good environment for me to study here.

Specially Dedicated

to my Parents,

“MR & MRS. MUZAFFAR HUSSAIN SHAH BUKHARI”

and Siblings

MOHSIN BUKHARI

HUMA BUKHARI

HAMMAD BUKHARI

HAMID BUKHARI

For encouraging and backing me to go on every

adventure specially this one, and supporting me either financially and morally at every stage.

ABSTRACT

Buckyball comprised of 60 carbon atoms is a nanoparticle (0D), which is arranged in a hollow interior with a spherical shape. MXene's hydrophilic surfaces with strong metallic conductivities stand out from the rest of 2D materials, such as graphene. MXene and C60 were both discovered to be appealing for super capacitors (SC), which are regarded replacements to energy storage devices due to their greater rate of charge/discharge over batteries. C60 and MXene both have surprising results in energy storage devices individually.

This thesis report is the study of the effect on capacitance of supercapacitor by variation of different concentrations of MXene and C60 in the nanocomposite. MXene was obtained from MAX by etching process at optimized parameters. C60 and MXene based nanocomposite were chemically synthesized by hydrothermal process at optimal conditions and characterised by X-Ray diffraction, scanning electron microscopy, energy dispersive spectroscopy, RAMAN spectroscopy and cyclic voltammetry. The structural properties by XRD results confirmed the successful etching of MXene from MAX and formation of nanocomposites comprises of MXene and C60. Surface morphological analysis revealed that Buckyball structure attained successfully with layers of 2D layers of MXene. Vibrational modes of C60 and MXene are confirmed by RAMAN spectroscopy which shows that the peak intensity of Ti_3C_2 bond is reduced with increase in MXene concentration. Electrodes are fabricated by different concentrations of MXene and C60 nanocomposites and Current-Voltage (I-V) measurement are performed at different scan rates to analyze the capacitance of pseudo supercapacitor which shows that capacitance is increased linearly with decrease in scan rate.

From the results and observations during experiments and calculations confirms that capacitance will enhance with higher concentration of MXene rather than C60. By virtue of all I-V measurements it is confirmed that nanocomposite having composition 90% and 10% of MXene and C60 respectively shows that capacitance is increased from 200 – 250 Fg^{-1+} (for pure MXene) to 348 Fg^{-1}.

Keywords: MXene, 2D Materials, Buckyball, C60

TABLE OF CONTENTS

LIST OF FIGURES

LIST OF TABLES

Chapter 01

1. INTRODUCTION

1.1 Energy Storage devices

Energy storage systems include components such as fuel cells, batteries, and capacitors to store energy in a variety of methods, including electrochemical, chemical, and thermal. When it is convenient, an energy storage device allows you to harvest heat or electricity from a renewable energy source and store it for later use. Thermal stores, electric batteries, super capacitors, and capacitors are among the most prominent energy storage devices. Types of energy storage devices are as under:

1.1.1 Super Capacitor

Researchers are interested in super capacitors (SCs), also known as ultra-capacitors, as high-performance energy storage technologies that can contribute to the rapid rise of low-power electronics (such as wearable and portable electronic devices) and high-power military usage (e.g., guided missile technologies). The electrochemical properties of SCs formed by mixing electrode and electrolyte materials can be utilised to evaluate their performance. Similarly, the selection of such materials can have a significant influence on the charge storage capacity of SCs.

1.1.1.1 Difference between characteristics of capacitor and super capacitor

Capacitors and supercapacitors have different properties and characteristics according to different parameters such as construction, materials used, charging and discharging time etc. Table 1-1 depicts the comparison chart between capacitors and supercapacitors in term of different parameters construction, materials used, charging and discharging time etc.

Table 1-1: Comparison of Capacitors and Super Capacitors

Characteristics	Capacitor	Super Capacitor
Construction	Two metallic terminals (Electrodes) device with dielectric medium in between. Electric energy is stored in the electrostatic field in it.	Type of polar capacitor and electrolytic solution is used instead of dielectric. The activated carbon is used on electrodes to enlarge the area.

Dielectric Material	Aluminium oxide, polymer films or ceramic are used as dielectric medium in between the electrodes.	Activated carbon is used as medium. Voltage applied; a double electric field is generated which acts like a dielectric medium.
Charge / Discharge Time	10^{-12} sec to 10^{-3} Sec	10^{-3} sec to 1 sec
Charge / Discharge Efficiency	> 0.95	0.85 – 0.98
Operating Temperature	-20 to 65 °C (-4 to 149°F)	-40 to 65 °C (-40 – 149°F)
Energy	<0.1 W h/kg	1-10 W h/kg
Advantages	It avoids excessive drawing of power Less Battery drain due to a capacitor High Integration Density Real/Reactive Power Control	Long Life Cycle High Energy Storage Fast Charging and Discharging Time High Load Currents

The space between electrolytic capacitors and rechargeable batteries is filled by super capacitors, which can frequently carry 10 to 100 times more energy per unit volume or mass than electrolytic super capacitors. Because they have working voltages ranging from 1V to 3V for both organic and aqueous electrolytes, super capacitors have significant promise for rapid charging and energy storage. In contrary to lithium-ion batteries, which degrade with each charge cycle, they have nearly limitless charge cycles.

1.1.1.2 Working Principle of a Super capacitor

A super capacitor's primary working principle is the storage of electrical energy within two electrostatic double layers formed when small layers of charge are formed on the boundary here between electrolyte and the inner surface of the capacitor electrode plates. Figure 1-1 depicts the mechanism of electric double layer capacitor.

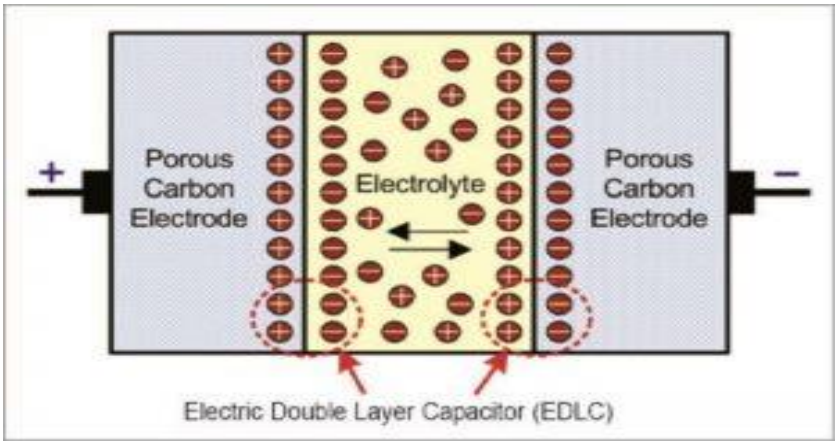

Figure 1-1: Mechanism of electric double layer Capacitor (EDLC).

1.1.1.3 Construction of a Super capacitor

A super capacitor is constructed in the same manner as a standard electrolytic capacitor. It is comprises of two metal electrode plates that are isolated by a small insulating material and immersed in an electrolyte solution. Super capacitors have conductivity plates with a significantly bigger surface area and plates that are placed closer together than normal capacitors. A super capacitor, while an electrochemical device, does not create power by chemical processes.

Porous materials such as carbon, activated charcoal, and others are typically covered upon this metal plates used to produce super capacitors. The electrolyte material inserted between the two plates provides the device with mandatory insulation and safety against short circuit and charge escape. A super capacitor may keep a vast amount of charge value because its capacitance value is always perfectly proportional to the surface area of its conduction plates, which in this scenario is quite huge. Furthermore, because super capacitors have significantly closer plates than regular capacitors, capacitance is inversely related to plate distance.

1.1.1.4 Working of a Super capacitor

To store energy, capacitors use electrostatics or static electricity. Ions that are both positively and negatively charged are discovered between the two plates of the super capacitor's electrolyte solution. When a voltage is applied between the plates of a super capacitor, one of the plates normally gets a +ve charge while the other plate accumulates a -ve charge. As a result, the positively charged metal plate attracts positively charged ions in the electrolyte solution, whereas the negatively charged metal plate attracts negatively charged ions. A small layer of ions is developed on the upper walls of both plates.

As a result, an electrostatic double layer forms, which is like connecting two capacitors in series. Each of the two resulting capacitors has a high capacitance value because the space between their charge layers is relatively small. Calculate the super capacitor's total capacitance by dividing (C1 x C2) by (C1 + C2).

1.1.2 Li-ion Battery

Lithium-ion batteries are a type of rechargeable battery that transfers lithium ions to the positive electrode form the negative electrode when discharge and back again during charging.

Alessandro Volta created the first cell more than 20 years ago using the idea of electrochemical potential. The periodic chart contains some of the best elements for use in batteries. The concept behind a cell based on electrochemical potential of different elements which is as under in Table 1-2:

Table 1-2: Electrochemical potential for different elements

Element	Electrochemical Potential
Li	3.04V
Mg	2.37V
Al	1.66V
Zn	0.76V
Fe	0.44V
H	0V
Hg	-0.24V
Cu	-0.34V
Ag	-1.69V
F	-2.8V

Li has highest and F has least tendency to lose electrons. Over 200 years ago, Volta created the first battery using Zn and Ag as electrodes. Based on the same idea of electrochemical potential, SONY (a Japanese multinational conglomerate firm) later in 1991 produced the first profitable model of lithium ion battery.

Electronic Configuration of Li atom is shown in Figure 1-2 as under

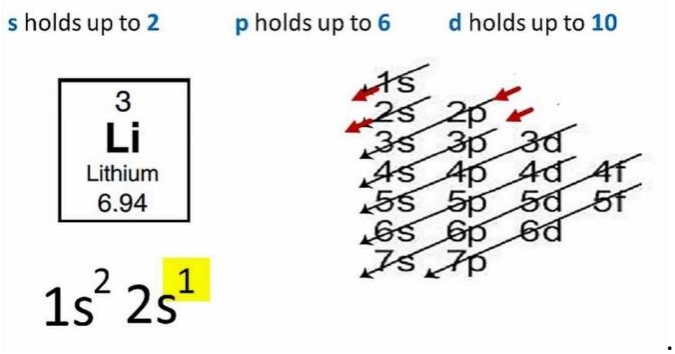

Figure 1-2: Electronic Configuration of Li atom

Because it only one electron in the outermost shell, lithium is an extremely reactive metal that reacts with water and air. While lithium is a reactive metal when pure, it is very stable when present as lithium oxide. A lithium ion battery contains a graphite layer and an electrolyte. Because the graphite layers are only weakly linked together, solitary lithium ions may be easily retained there. The electrolyte acts as a barrier, enabling only lithium ions to pass through graphite and metal oxide. Schematic diagram of Li ion battery is shown in Figure 1-3.

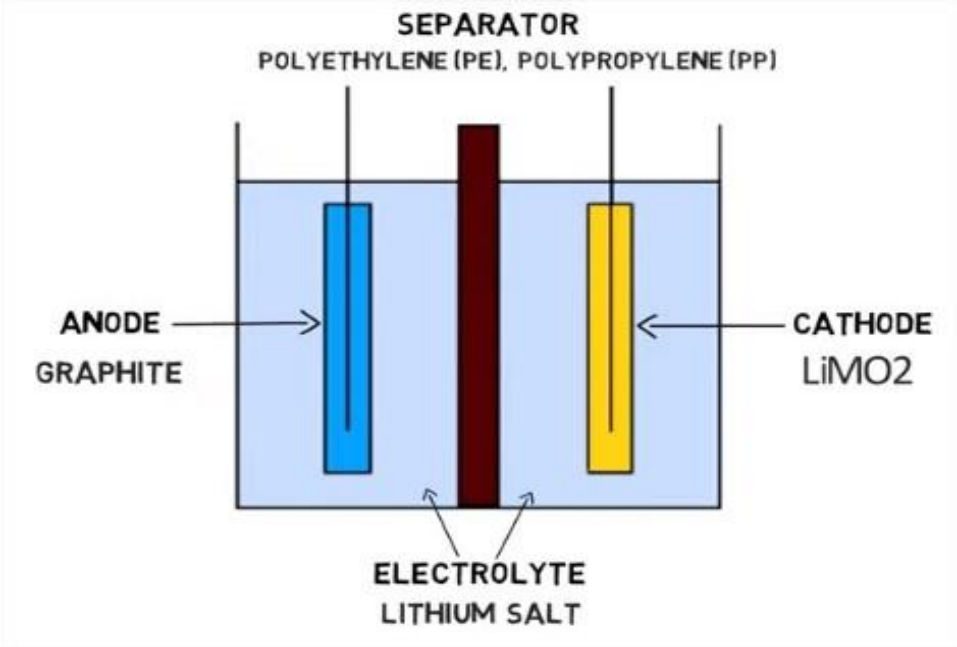

Figure 1-3: Schematic diagram of Li ion battery

1.1.2.1 Charging Process

When linked to a power source, the positive side draws and eliminates electrons from lithium metal oxide atoms. These electrons can move across an external circuit since they cannot pass it via

electrolyte and enter the graphite layer. However, positive lithium ions are driven to the negative terminal and travel through the electrolyte to the gap between the graphite layers, where they are trapped. After the lithium atom has travelled through to the graphite layer, the cell is fully charged. Charging principle of Li ion battery is shown in Figure 1-4.

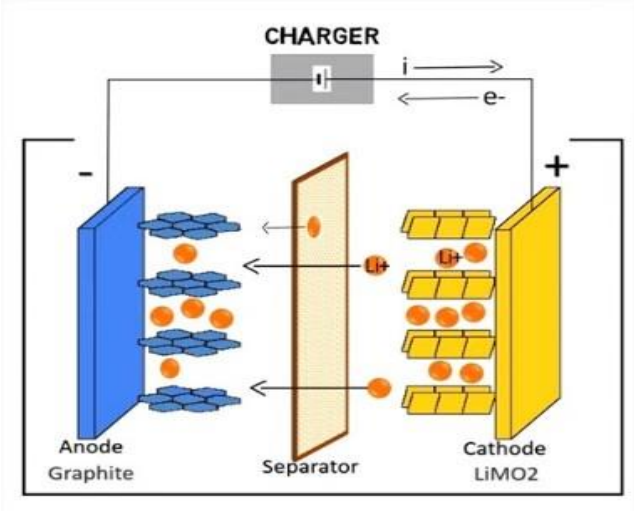

Figure 1-4: Charging principle of Li ion battery

At Cathode:

$$LiMO_2 \rightarrow Li^+ + MO_2 + e^-$$

At Anode:

$$C_6 + Li^+ + e^- \rightarrow LiC_6$$

Cell Reaction:

$$LiMO_2 + C_6 \rightarrow MO_2 + LiC_6$$

1.1.2.2 Discharging Process

During the charging process, the lithium ion and electrons were isolated from the metal oxide, which was the primary aim because lithium is unstable in this state. Turn off the power source before connecting the load.

As a result of their desire to revert to their stable state as a component of metal oxide, lithium ions travelled to the electrolyte and electrons via load. This is how we get electrical current via the load. Graphite has no participation in the chemical processes of lithium ion batteries. It simply acts as a storage medium for lithium ions. Discharging principle of Li ion battery is shown in Figure 1-5.

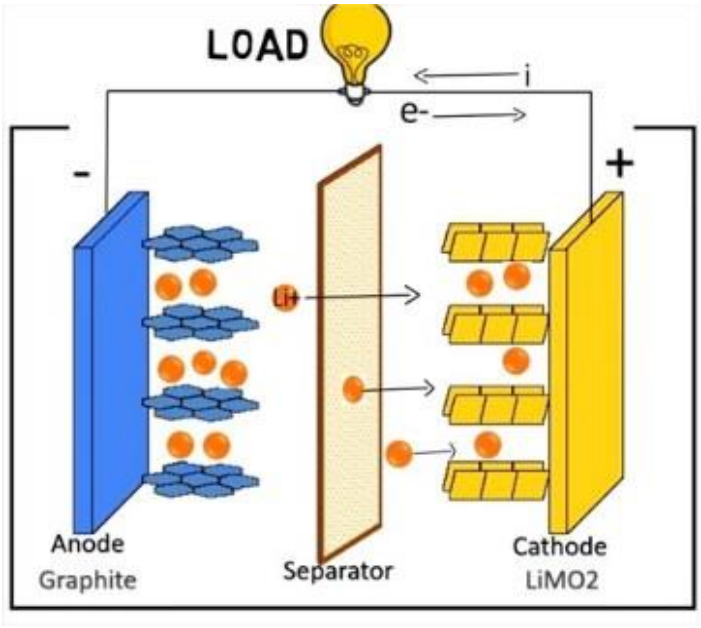

Figure 1-5: Discharging principle of Li ion battery

At Cathode:

$$MO_2 + Li^+ + e^- \rightarrow LiMO_2$$

At Anode:

$$LiC_6 \rightarrow C_6 + Li^+ + e^-$$

Cell Reaction:

$$MO_2 + LiC_6 \rightarrow LiMO_2 + C_6$$

If the outside temperature increases owing to a critical circumstance, the liquid electrolyte will run dry, resulting in a short circuit between the cathode and anode. This can result in a fire blast. For this, a non-conducting layer called separator is inserted among the electrodes. By virtue of its tiny porosity, the separators is permeable to lithium ion.

Graphite and metal oxide were deposited on copper and aluminium foils in practise. The foil serves as a current collector, and organic lithium salts serve as an electrolyte. It is covered in individual sheets. All of these sheets are coiled into a cylinder around with a central steel core, resulting in a more compact cell.

1.1.2.3 Upcoming research in Li-ion Batteries

Currently, the number of charge and discharge cycles for lithium ion batteries is approximately 3000. Researchers and scientists are working hard to get it up to 10,000 cycles. It means you won't have to worry about replacing your batteries for any devices for the next 25 years. Scientists are working to replace graphite as a storing media with silicon. This method will more than fivefold the energy density of Li-ion batteries.

1.1.3 Fuel Cells

A fuel cell is a galvanic cell that converts the chemical energy of a fuel-oxidant system directly into electrical energy. A fuel cell contains two electrodes and an electrolyte. The fuel and oxidant are continually and independently carried to the cell's two electrodes.

Sir William Grove (1839) created the first fuel cell. He utilised a platinum (Pt) electrode with the reactants H2 and O2. The electrodes are porous, allowing for a huge surface area. Heat is only partially transformed into mechanical energy, whereas in a fuel cell, chemical energy is totally converted into electrical energy (100% efficiency). Fuel cells utilise both liquid (methanol, ethanol, hydrazine, formaldehyde) and gaseous (hydrogen, alkane, carbon monoxide) fuels. Oxidants such as O2, air, H2O2, and HNO3 are used. Pt, porous PVC, nickel boride, Raney nickel, and Teflon were employed as electrodes. Finished in silver.

Fuel cell classified on the basic of temperature are:

- Low Temperature Cell ($<100^0$ C)
- Medium Temperature Cells (100 -2500^0C)
- High Temperature Cells ($>500^0$ C)

1.1.3.1 How Fuel Cell Works

A fuel cell's purpose is to produce an electrical current that can be routed outside the cell to conduct function, like providing power to an electric motor or lighting a city. Because of the characteristics of electricity, this current returns to the fuel cell, complete an electrical circuit. The chemical processes that produce this current are essential for the working of a fuel cell.

There are several varieties of fuel cells, each with its own set of characteristics. In general, hydrogen atoms enter a fuel cell at the anode and are chemically stripped of their electrons. The

hydrogen atoms have been "ionised," giving them a positive electrical charge. To accomplish labor, negatively charged electrons transport electricity across wires. If AC is needed, the DC output of the fuel cell must be routed through a conversion instrument called as an inverter. The oxygen is transferred the fuel cell at the cathode. The electrolyte is essential. It must only enable the required ions to pass between the anode and cathode. If free electrons or other materials could traverse the electrolyte, the chemical reaction would be disrupted. Hydrogen and oxygen combine, whether at the anode or cathode, to produce water, which flows out the cell. A fuel cell will generate electricity as long as it is fed hydrogen and oxygen. Even more, because fuel cells create energy chemically instead of through combustion, they are not limited by the thermodynamic principles that limit typical power plants. As a consequence, fuel cells collect more energy from their fuel in a more efficient manner. Extra heat from specific cells can also be utilised, further enhancing system efficiency. Figure1-6 depicts the working concept of a fuel cell.

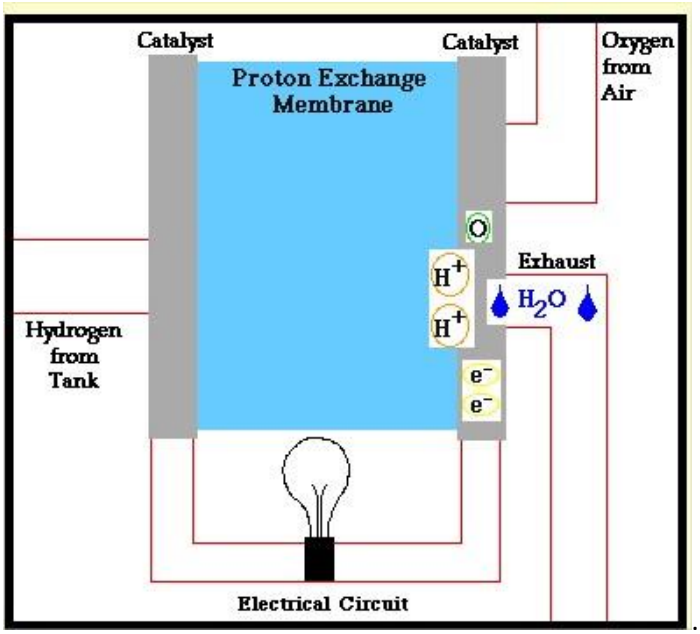

Figure 1-6: Working principle of Fuel Cell

1.1.3.2 Equations for chemical reactions in Hydrogen – Oxygen Fuel Cell

At Anode:

$$H_2 \rightarrow 2H^+ + 2e^-$$

At Cathode:

$$\frac{1}{2} O_2 + 2H^+ + 2e^- \rightarrow H_2O + \text{Heat}$$

Overall Reaction:

$$H_2 \rightarrow 2H^+ + 2e^-$$

$$\frac{1}{2} O_2 + 2H^+ + 2e^- \rightarrow H_2O + \text{Heat}$$

$$\frac{1}{2} O_2 + H_2 \rightarrow H_2O + \text{Heat}$$

1.2 Introduction of Super Capacitors

Super capacitors may store a high quantity of energy, often 10 to 100 times extra energy per unit mass or volume as compared to electrolytic capacitors. It is chosen over batteries due to its quicker and easier charging and charge delivery. A super capacitor may also be referred to as an ultracapacitor or a double-layer electrolytic capacitor. It can offer high energy and allow for huge load currents because to its low resistance. Its charging method is fast and easy, and it never overcharges. In comparison to a battery, a super capacitor provides greater low- and high-temperature charge and discharge performance. It's also quite reliable and has a lower resistance.

1.2.1 History of super capacitor

Super capacitors begin to fill the void between such a battery and a capacitor. The idea of a "super capacitor" is not novel. In truth, General Electric Co. built the first super capacitor device in 1957 (General Electric Company is an American multinational company incorporated in New York State and located in Boston), although there are no known commercial uses.

When working on fuel cells in 1966, Standard Oil Firm (an American oil producing, transport, refinery, and marketing company) developed the double-layer capacitor by accident.

NEC (Nippon Electric Company, Limited) of Japan started commercially supplying the initial "super capacitor" for memory storage backup in the late 1970s. In truth, while many devices are widely referred to as "super capacitors" or "ultra-capacitors," the labels are interchangeable and actually rely on what the firm making it wants to call it. For the most part, it's merely a trademark issue.

Products used as a starter for diesel trains began to reach the market in the 1990s, pushing the frontiers of storing energy and capacitor applications. The super capacitor market is dominated by companies such as Maxwell Technologies, Murata, and Tecate. However, new advancements in graphene based capacitors are reviving the rise of super capacitor efficiency and usage.

Super capacitors, however, cannot match with Li-ion batteries in terms of high specific energy and long-term energy storage. Nonetheless, several businesses are making headway on initiatives that will making super capacitors more widely usable.

Super capacitors, although superior to standard capacitors in terms of energy storage and release, cannot substitute the function of normal Li-Ion batteries. Specifically, Li-ion batteries outperform supercapacitors in terms of specific energy or energy density (Li-ion 250Wh/kg vs. Ultra-capacitors 20Wh/kg). Even firms focused on super capacitor technology, such as Skeleton Technologies, concede that a hybridization of Li-ion and super capacitor powered power systems might usher in the next era of electric technology. And, in truth, the majority of the products we see today. Ragone plot of energy storage devices is shown in Figure 1-7.

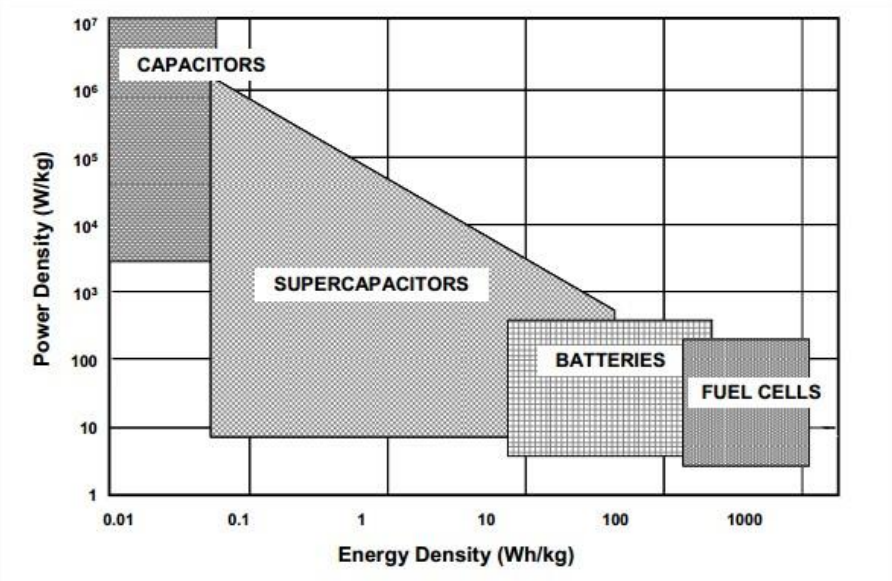

Figure 1-7: Ragone plot of energy storage devices [3]

1.2.2 Types of Super Capacitors

There are three type of Super Capacitors shown in Figure 1-8:

- Electrostatic double-layer capacitors (EDLC).

- Pseudo-capacitors.
- Hybrid capacitors.

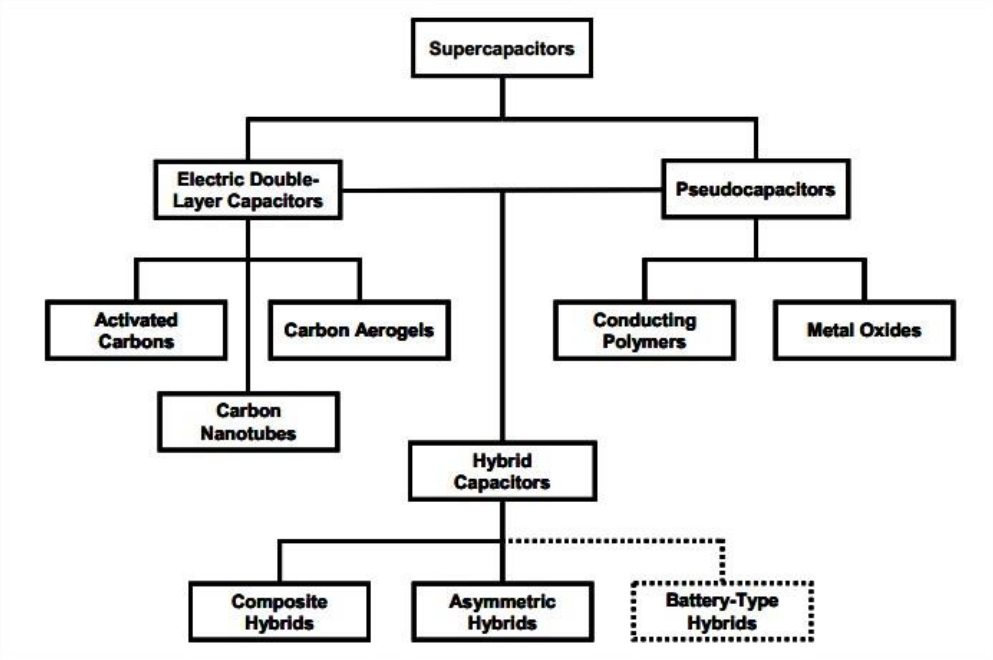

Figure 1-8: Types of Super Capacitors

1.2.2.1 Electrostatic double-layer capacitors (EDLC)

The electric double layer that exists at the contact between such a conductor and its interacting electrolyte solution formed the basis for the early notion of an electrochemical super capacitor. Hermann von Helmholtz suggested the electric double-layer hypothesis, which was further improved by Gouy, Chapman, Grahame, and Stern.

Electrochemical double-layer super capacitor (ELDCs) are made up of two carbon-based electrodes, an electrolyte, and a separator. ELDCs, like conventional capacitors, may store charge electrostatically or non-Faradaically between electrodes. There really is no charge transfer between the super capacitor's electrodes and electrolyte.

To store energy, ELDCs employed an electrochemical of charge. When a voltage source is given to electrodes, charges mix at the electrode surface due to the natural interaction of unlike charges (according to Coulomb's electrostatic force of attraction). Ions in the electrolyte flow through the separation into the pores of opposite-charged electrode pores. The electrodes are constructed in

such a way that ion recombination is avoided. As a result, each electrode has a second layer of charges. Charge and Discharge of ELDCs is shown in Figure 1-9.

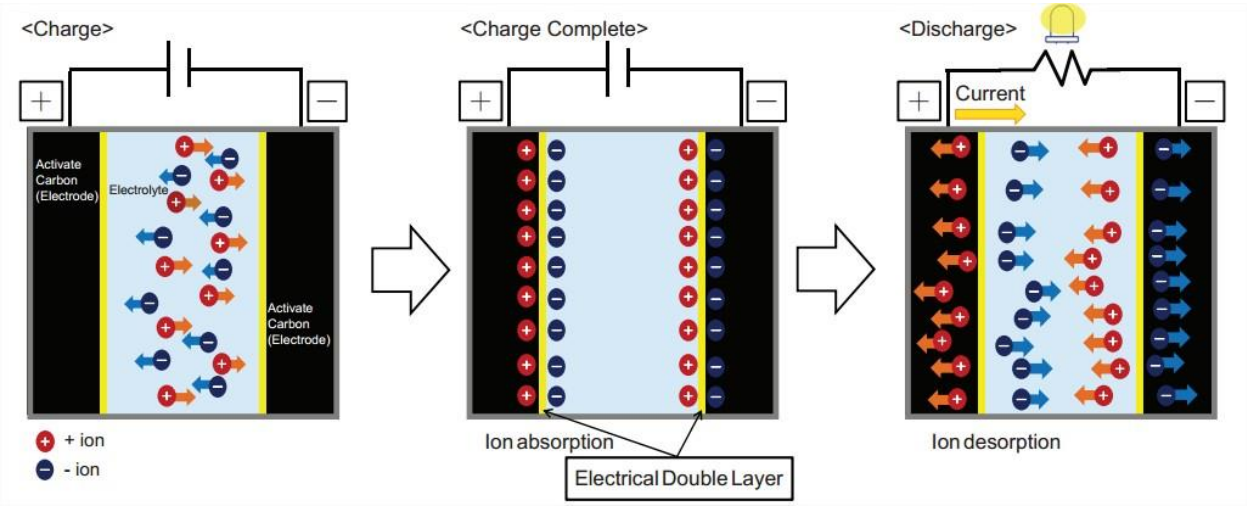

Figure 1-9: Charge and Discharge of ELDCs [5]

Super capacitor working based on previous conventional capacitor but the electrodes in super capacitors have much higher surface area and much higher thin dielectric that decreases the gap (D) between the two electrodes as below equations:

$$C = \epsilon_0 \epsilon_r \frac{A}{D} \quad and \quad E = \frac{1}{2} CV^2 \qquad \textit{Equation 1-1}$$

ϵ_0 =Permittivity of free space,

ϵ_r = Relative Permittivity of dielectric,

A = effective area

Furthermore, by retaining low equivalent series resistance (ESR), quicker charging/discharging time, and long cycle life, super capacitors designed to reach high power densities outperform fuel cells and electrochemical batteries [1, 2].

Because there is no charge transmission between both the electrodes and electrolyte, there are no chemical changes related with the non-Faradaically process. Because of this, charge storage in ELDCs is more reversible, which allows for high cycling stabilities of roughly 106- cycles. Because of its cyclic stability, ELDCs are commonly employed in applications such as non-user serviceable places such as ocean depths or mountain environments. [3]. Charge Storage Mechanism is shown Figure 1-10.

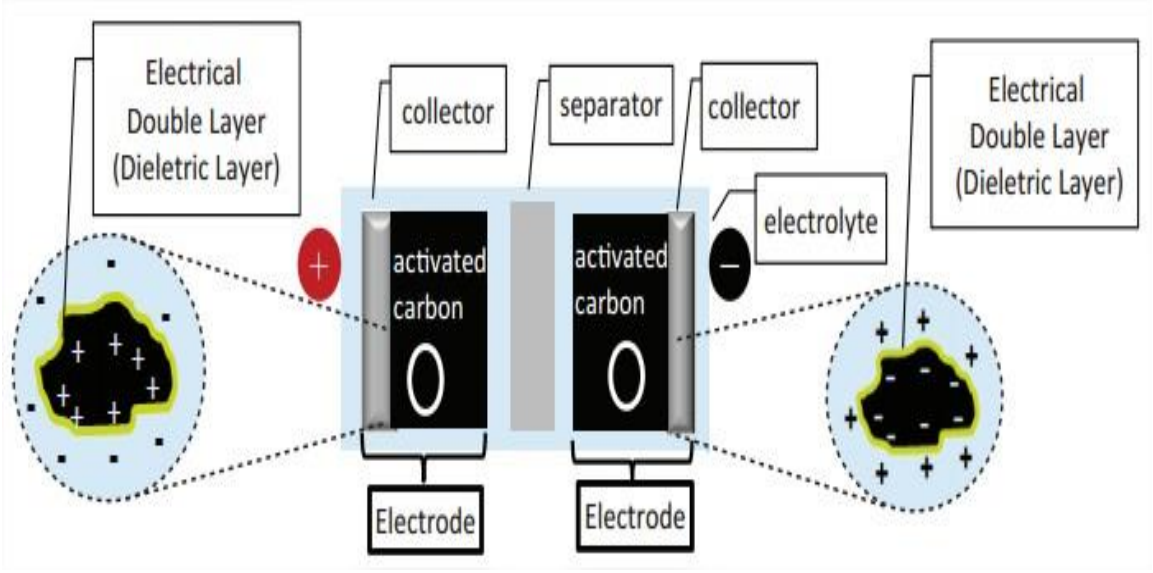

Figure 1-10: Mechanism to store charges [5]

Electrolyte and electrode in ELDCs

The energy density of a super capacitor might vary depending on the type of its electrolyte. In ELDCs, an aqueous or organic electrolyte can be employed. In comparison to organic electrolytes such as acetonitrile, aqueous electrolytes such as H2SO4 and KOH have lower ESR (Equivalent series resistance) and need a smaller minimum pore size. Aqueous electrolytes exhibit a low voltage breakdown as well. The electrolyte of choice is also determined by the intended uses.

Carbon electrodes have a larger surface area, are less expensive, and use more advanced processes than other materials such as metal oxides (MO) and polymers. Carbon materials like as carbon nanotubes, carbon aerogel, and activated carbon are employed as electrodes in ELDCs [2].

Activated Carbon

To achieve a high effective surface area, activated carbon employs a complicated porous structure composed of variable sized microspores (20 wide), mesopores (20 - 500), and macrospores (>500) [4].

However, capacitance is closely connected to surface area, but not all surface area contributes to capacitance in activated carbon. This is generated by electrolyte ions that seep into microspores, preventing some of the pores from participating in charge storage. [5]. Large pore sizes correspond to high power densities, while tiny pore sizes correspond to high energy densities [6].

Carbon Nanotubes

Carbon nanotube electrodes are typically formed as an intertwined mat of carbon nanotubes with accessible and open mesopores structures Shown in Figure 1-11. Figure depicts this unique characteristic of CNTs. Like other carbon-based electrodes, carbon nanotubes are linked here, allowing for continuous charge distribution and the use of nearly the whole surface area to store charges. As a result, the surface area of CNTs is employed more proficiently to attain capacitance similar to activated carbon based super capacitors. [8].

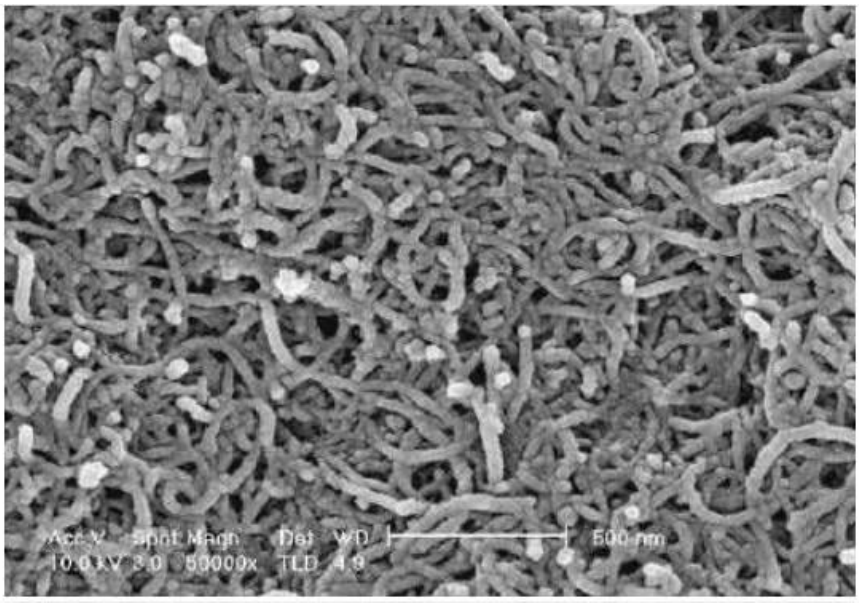

Figure 1-11: SEM image of entangled mat of carbon nanotubes [7]

1.2.2.2 Pseudo capacitors

Pseudo capacitors store charge faradaically by charge transfer between electrolyte and electrode. This was accomplished using a redox reaction and an intercalation method [9]. The Faradaic reaction produces greater capacitance than ELDCs. These faradaic techniques may enable pseudo capacitors to obtain higher capacitance and energy levels. It involves a reduction-oxidation process, similar to that of batteries. As a result, it has poor cycle stability and a low power density. It is built similarly to EDLCs, however the electrodes are comprised of metal oxides or perhaps conducting polymers. As a result, it is not as permeable as EDLC [13].

Mechanism for Pseudo Capacitors:

Under potential depositions, reduction-oxidation processes, and the intercalation process are used to accomplish this. Under potential deposition happens when metal ions develop and absorb a

monolayer on certain metal surfaces that are substantially over their redox potential. Lead on the face of a gold electrode is a classic example of the under potential deposition [14].

Current collector with the ruthenium dioxide Nano cluster, then hydras grain boundary, and H+ ion from the electrolyte arriving and departing collected inside it. This process is taking place for the intercalation pseudo capacitance. Simply said, the substance over there is working as a composite. So, inserting complete materials is one type of doping of the material in this circumstance [12]. Figure 1-12 shows the e equivalent circuit Diagram and structure of pseudo capacitor.

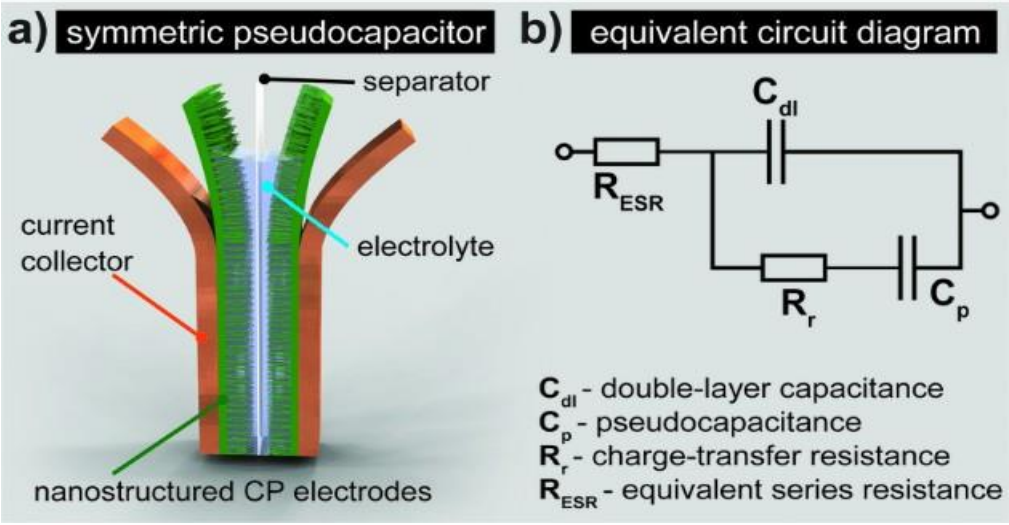

Figure 1-12: a) Construction of a pseudo capacitor cell b) Equivalent circuit diagram [11]

Materials for Pseudo Capacitor:

Conducting polymers:

Conducting polymers such as polyacetylene, polypyrrole, polyaniline, and poly 3, 4 ethylene dioxythiophene, sometimes known as PEDOT materials, have been identified as viable pseudo capacitive electrode materials for super capacitors. They provide capacitive behaviour via redox processes that take place on the interface and throughout the bulk.

Because no structural changes, such as phase transition, occur during redox reactions, they are extremely reversible. Because of their cheap cost, environmental stability, and ease of synthesis, these metals are the most attractive members. Conducting polymers can expand and contract

during the intercalation and de-intercalation processes, resulting in limited cycle stability when utilised in super capacitors [12]. Mechanism of store charge faradaically is shown in Figure 1-13.

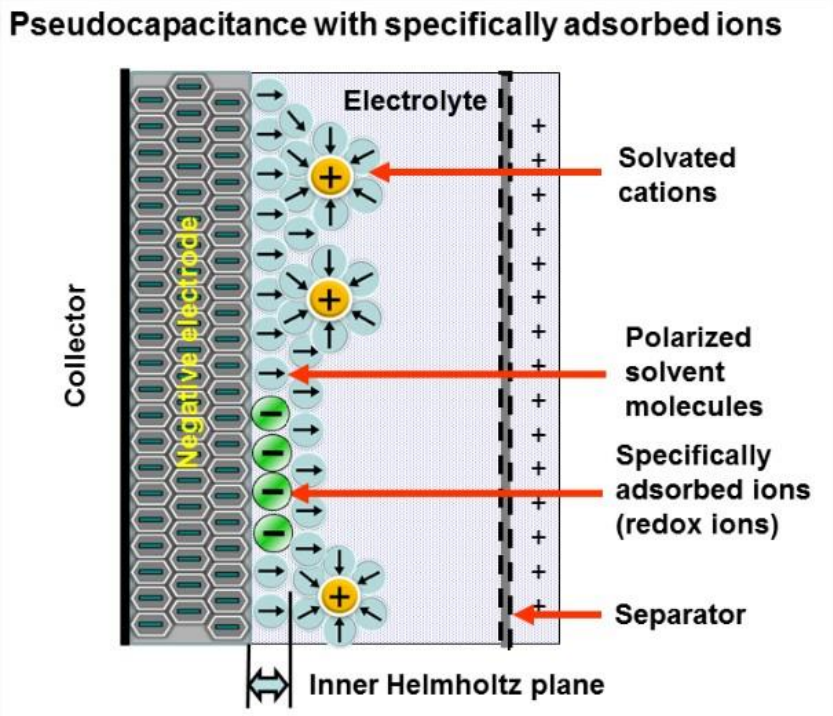

Figure 1-13: Mechanism of store charge faradaically [13]

Metal Oxides:

Metal oxides offer significantly greater spatial capacitance than carbon materials for EDLCs. Several metal oxides such as RuO_2.H2O, IrO2.H2O, MnO2.H2O, V2O5 (tin oxides), Fe2O3 (ferrous oxide), and certain hydroxides such as cobalt hydroxide, nickel hydroxide, or their composites have been extensively studied as pseudo capacitive electrode materials in recent years [11-13].

Many studies have also concentrated on mixing ruthenium oxide with low-cost metal oxides as SnO2, MnO2, NiO2, and CaO to generate composite oxide electrodes [14].

1.2.2.3 Hybrid capacitors

The storage concept of hybrid super capacitors is regulated by a mix of EDLCs and the pseudo capacitor storage theory. The pseudo capacitor lacks the restricting property of EDLCs and vice versa.

There are some benefits to the EDLC, but there are also some drawbacks. The same may be said with pseudo capacitance, which has both advantages and problems. Scientists are now incorporating both techniques in order to mitigate all of the downsides. The combining of EDLC and pseudo capacitor storage results in the overshadowing of the restrictions of the combining parts, with the advantage of giving larger capacitance, which is why it is referred to as the hybrid [14].

When made up of two separate electrodes constructed of different materials, hybrid super capacitors exhibit superior electrochemical behaviour than individual ones. In the EDLC instance, we used the identical anode and cathode materials. In this scenario, the anode and cathode materials are distinct. The researchers concentrated on three distinct forms of hybrid capacitors defined by their electrode designs, namely composite, asymmetric, and battery type. Schematic presentation of the electrochemical and electrostatic charge and discharge of the double layer and intercalation function in the synthesized hybrid super capacitor is shown in Figure 1-14.

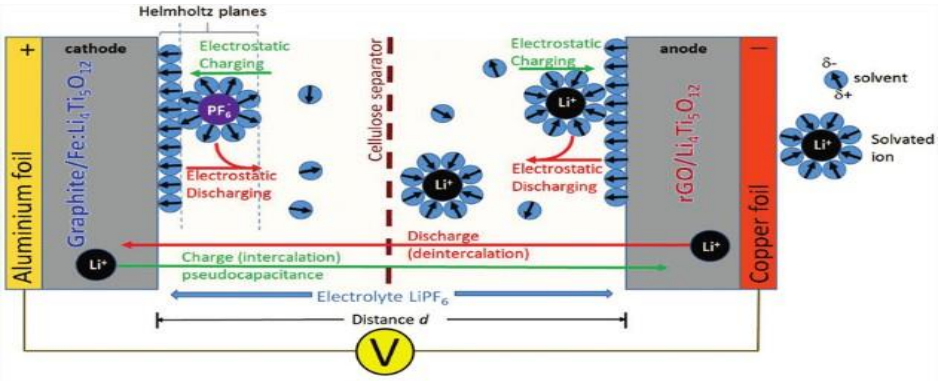

Figure 1-14: Presentation of the electrostatic and electrochemical charge and discharge of the DL and intercalation function in hybrid super capacitor [15]

Asymmetric hybrid

By linking and EDLC with a pseudo capacitors electrode, a non-faradic and faradic process is combined. They are designed in such a manner that the carbon material serves as the -ve electrode and either metal oxide or a conducting polymer serves as the +ve electrode [11-13].

Battery type

A hybrid electrode combines two distinct electrodes: a super capacitor electrode and a battery electrode. This structure was designed to take use of the features of both super capacitors and batteries in a single cell.

The most adaptable performance features of any super capacitor are found in hybrid super capacitors. It is suitable for a wide range of applications. Can reach extremely high energy and power densities while maintaining cycle stability and cost.

Electrolyte materials

The electrolyte, which contains solvent and salt, is one of the most important elements of electrochemical super capacitors because of the advantages of ionic conductivity and charge levelling on both electrodes of the cell. So it is essentially a mixture of the electrode and the electrolyte component.

1.2.3 2-Dimensional Martials for Super capacitors

The material used to make the electrode for a super capacitor is critical for increasing electrochemical parameters such as specific capacitance, energy density, cyclic stability, and power density. Two-dimensional materials have emerged as a potential material for SC electrodes. Many unique features of 2D materials and combinations of 2D materials have raised their appeal for SCs. Many different forms of 2D materials are discussed, including MXene, metal organic frameworks (MOFs), transition metal dichalcogenides (TMDs), transition metal chalcogenides (TMCs), metal nitrides (MNs), covalent organic frameworks (COFs), and black phosphorus (BP).

1.2.3.1 MXenes

Yury Gogotsi [16] in 2011 synthesized the MXenes material initially. MXenes are a kind of 2D chemical compound known as the MAX phase. It is designated as Mn+1 A Xn, where M is a transition metal (e.g., Nb, Sc, Ti, Cr, Zr, Mo,V Hf), X is nitrogen, carbon, and A is a group XIII or XIV element (such as Sn, Al, and Si) [17].

MXene is a unique material composed of transition metal nitrides, carbonitrides, and carbides that is created by removing a specific element from its multiple layered structure by etching the element A from the MAX [18, 19]. Removal of a required element from their multiple layered structure through etching the element A from the MAX shown in Figure 1-15.

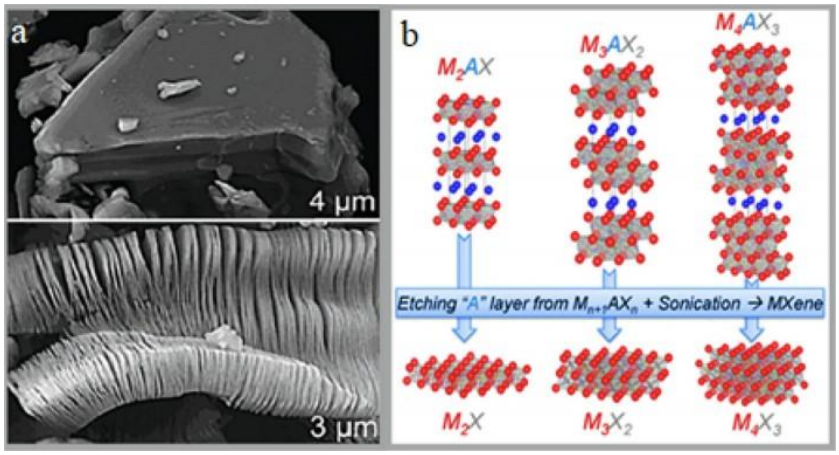

Figure 1-15: Removal of a required element from their multiple layered structure through etching [20]

By virtue of their unique mix of hydrophilic nature and metallic conductivity, MXenes have shown to be amazing featured materials in energy storage devices, particularly for electrodes of SCs applications [21]. There are several varieties of MXene available, including Ti2CTx, Ta4C3Tx Ti3C2Tx, Nb4C3 Tx, Nb2CTx, V2CTx, and Ti2NTx MXene. Because of their ability to store charges via pseudo capacitive processes, these new materials can be employed as electrode materials for SCs [22, 23].

Qiu et al. synthesised Ti3C2 MXene using several techniques and measured its conductivity to be 260 Scm-1. This conductivity value for Ti3C2 MXene is more than that of rGO, which has a conductivity of around 1 Scm-1 [24]. The electrical conductivity of Ti3C2 MXene layers formed by spin-casting has been reported to be up to 6500 Scm1, which is higher than the electrical conductivity of most two-dimensional materials [25].

One of the crucial characteristics is the coalescence of multivalent ions such as Al3+, Zn2+, Mg2+, and big organic ions. Optimizing the ion movements among MXene layers yields a more power in Scs, allowing MXene-based SCs with low R to change electrolytic capacitors [25]. Zhang et al. [22] created a conductive and extremely bendable electrode by layering MnO2 and MXene over carbon fabric. In compared to MnO2 Nano rods/carbon fabric, the resulting electrode has a higher capacitance of about 511.2 Fg^{-1}.

However, the energy and power density of an asymmetric flexible device consisting of MnO2 Nano rods, MXene, and carbon fabric were 29.58 Whkg-1 and 749.92 Whkg-1, respectively. With such high conductivity and energy density, MXene also has the benefit of having good mechanical

and chemical resilience [18]. The structure and conductivity of reactive electrode materials may be improved using effective interfacial engineering approaches.

The organic asymmetric super capacitor's gravimetric and volumetric cell capacitances were 30 Fg-1 and 41 Fcm-3, respectively, which were higher than the symmetric cells made of Ti3C2Tx and rGO. In comparison to the asymmetric aqueous device, the potential window and, as a result, the energy content of the asymmetrical super capacitor with electrolytes provided greater values [26].

Also, Rakhi et al. [27] have synthesized the Nano crystalline MnO2 directly on MXene Nano sheets using a facile chemical. Presentation of different kinds of 2D nanomaterial's for electrode materials in super capacitors as shown in Figure 1-16.

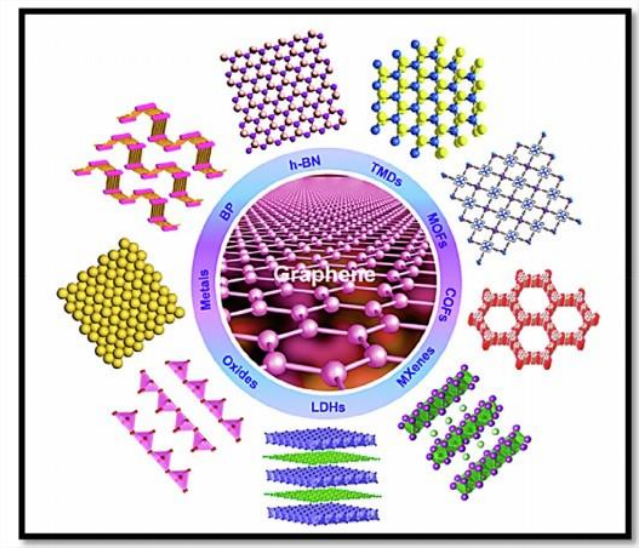

Figure 1-16: Presentation of different kinds of 2D nanomaterial's for electrode. *[25]*

1.2.3.2 Graphene

Because of its unique chemical and physical characteristics, graphene has been effectively used as an electrode. Rouff et al. [26] proposed turning graphite directly into graphene oxide (GO) by chemical modification for use as a supercapacitor electrode. Graphene specific capacitances were 99 and 99 F g1 in resulting and aqueous solutions, respectively.

A chemical upgrade of graphene, which has a huge surface area and electrical conductivity, might be a promising choice for EDLC ultracapacitors, according to Rouff et al [26]. Graphene-based ultracapacitors may be inexpensive and efficient enough to be used in a variety of energy storage

applications. Since then, various research teams have looked at the direct usage of graphene and its mixtures in supercapacitors.

117 Fg^{-1} was the electrical double layer capacitance of graphene produced by exfoliating graphite with an acid combination and then thermally decreasing it. Exfoliated graphene has a much greater capacitance than nanodiamond (35 Fg^{-1}) and camphor graphenes (6 Fg^{-1}). To widen the potential window value, they continued their experiment by employing an ionic liquid as an electrolyte. The ionic liquid's active component (exfoliated graphite) has a specific capacitance of 75 F g1 and an energy density of 39 W h kg^{-1}.

In this condition, the reducing agent urea greatly decreases the oxygen functional groups on the basal plane and at the GO edges. The resultant RGO had specific capacitances of 255 and 100 Fg^{-1}, respectively, at current densities of 0.5 and 30 Ag^{-1}, with an estimated capacity retention of 93% [27]. Furthermore, due to a porous network and a partially recovered -conjugation structure, they attained a relatively high specific capacitance compared to RGO generated using hydrazine reduction and hydrothermal procedures.

1.2.3.3 Transition metal dichalcogenides (TMDs)

TMDs have the crystal structure formula MX2, where M may be any transition metal element like Ti, Mo, V, Re, or Ta and X can be any chalcogenide element like S, Se, or Te. The van der Waals force holds TMD monolayers together, and each layer is made up of 3 atomic layers, with a transition metal layer sandwiched between two chalcogen sheets [28].

TMDs with multilayer structures akin to graphite and the early relatives of graphene, such as TiS2, MoS2, TaS2, and NbSe2, exhibit the same flexibility, slimness, and transparent as graphene [29]. Unlike graphene, many 2D-TMDs are designed as semiconductors and hence have a significant potential for development into ultra-small, low-power transistors with better performance than silicon-based transistors.

Because of their extraordinary physicochemical qualities, including as wide surface area, strong catalytic activity, amazing semiconducting capability, low price, high chemical durability, and high tensile capabilities, TMDs have attracted a lot of interest as electrode materials. Mechanical exfoliation, fast supercritical fluid extraction (in solvents, chemical vapour deposition (CVD), as well as other pretreatment techniques [30, 31] are used to facilitate their manufacturing.

Due to their thin atomic profile, which produces ideal conditions for higher electrostatic effectiveness, a controllable electronic structure, mechanical strength, optical transparency, and sensor sensitivity, 2D-TMDs are useful materials used in a broad range of fields, such as sensing photonics, electronics, and energy devices [30,31] such as sensors, optical displays, transistors, and supercapacitors.

MoS2 may be used in flexible electronic devices, optoelectronic devices, and composite films due to its remarkable elastic characteristics in both single-layer and multi-layer forms [33]. 2D layered implementations have substantially enhanced in the field of energy storage development due to their superior structure with interspace among layers and high surface area, which allows for simpler intercalation for small molecules and ions and results in reversible and swift redox reactions [34].

Several studies [35, 36, and 37] have concentrated on the hybridized 2D-TMDs with various carbon-based supporting materials in order to enhance active sites and boost charge transferability. Furthermore, the electrochemical supercapacitor performance of a VSe2/RGO hybrid, whose hybrid supercapacitor was made in a single step, was reported for the first time.

1.2.4 Zero Dimensional (0D) Materials for energy storage devices

The majority of contemporary electrochemical capacitor research is concentrated on power and energy density, as well as the use of environmentally acceptable materials [39]. As according Chang et al. [39], hydrous RuO2's Nano tubular array architecture offers highly specific capacitance and excellent reversibility, but its practical use is limited by its high cost and toxicity.

After establishing that C60 could collect photo - induced electrons both from conjugated polymers and its heterostructures, Sapurina et al. [41] joined fullerene C60 and linked polymers to make composites. Due to its remarkable redox capabilities, unique proton doping process, significant ecological stability, and low cost, PANI is the most common conjugated polymer and is considered as one of the best supercapacitor electrode materials.

Polyaniline has a theoretical maximal capacitance of up to 2000 Fg -1. Moreover, there is a large decrease as a result of its weak conductivity and electron transfer efficiency. Furthermore, polyaniline has a physical degradation concern, making it an excellent material for just a single

electrode [42]. As a result, making composites out of polyaniline and carbon is a preferred solution to this problem.

Fullerene C60 is a carbon molecule with a unique p-electron conjugated structure that gives it a high electrochemical potential [43]. PANI has a low doping level, to the greatest of our knowledge. The current work involves the direct mixing of FW/toluene solution and PANI-EB/N-methyl-2-pyrrolidone colloid to produce an FW/PANI-EB composite with corrugated surface shape. A novel FW/PANI-EB composite showed a high specific capacitance and a long cycle life.

Once the current density is 1 Ag-1, the capacitance of the FW/PANI-EB mixture is 813 Fg-1, whereas polyaniline is 248 Fg-1, and the composite's holding is 85.2% after 1500 cycles. The FW/PANIEB composite performs admirably as a supercapacitor. A comprehensive suggestion for the assembly technique that results in the curved surface of the FW/PANI-EB composites is also made. At a current density of 1 Ag-1, the capacitance of the FW/PANI-EB composite with corrugated surface shape is as high as 813 Fg-1. The capacity retention of the composite after 1500 cycles is 85.2%. (693 Fg-1) Specific capacitance

Notably, the regular arrangement of fullerene molecules has the potential to systematically regulate or significantly improve the properties of fullerene micro/ nanostructures (FMNSs) [44, 46]. By combining fullerenes with other moiety, such as metal-porphyrins [47] and carbon nanotubes (CNTs) [48], a distinct technique has generated a variety of advantageous hybrids or composites.

1.2.5 2D/0D composite based Supercapacitors

Combining Nano scale and pseudo capacitive materials is one of the most effective methods to boost the conductivity and cycle steadiness of metal oxide through synergistic effects [51]. Significant efforts have been made to capitalise on this relationship.

Designing and improving nanostructured electrode materials for supercapacitors has lately gained more attention, particularly [52]. Several studies have been conducted on various types of nanomaterials. Nanomaterials are often classified as 0D, 1D or 2D.

0D nanostructures are particles with 3 Nano scale-prohibited dimensions (usually 1-100 nm). Nano rods and nanotubes are frequently identified in 1D nanostructures based on the length/diameter ratio. 2D materials frequently feature two extra dimensions that are bigger than the Nano metric

dimension, in addition to a few atomic layer thickness. Carbon nanostructures of different diameters that can be employed in EDLCs include activated carbon, CNTs, graphene, and carbon generated from carbides. CNTs have a unique form with a tubular porous structure to improve electron and ion transit and boost the energy density of supercapacitors [53].

Etching and delamination operations are critical when developing MXene-based materials [54]. Supercapacitors can be doped with heteroatoms (such as N or S) to increase their capacitance [55]. Chemically addition of impurities with different elements such as nitrogen and boron is one of the most effective ways to improve the electrical properties of graphene [56].

Comparable research has been undertaken on 1D materials. Zhu et al. [57], for example, generated N-CNTs/MnO2 composites with a high capacitance of 366.5 F g1 at a current density of 0.5 Ag-1. MnO2 Nano sheets were grown in situ on N-CNTs to generate N-CNTs/MnO2 Nano composites. As a result, this Nano composite retains 86.8% of its capacitance after 1000 cycles and has a specific capacitance of 219 Fg-1 at a current density of 1.0 Ag-1 [58].

Because of its high conductivity, high capacitance, and ecological friendly, MoO2 is a good choice for positive electrodes [60, 61]. The RGO.MoO2/C, for example, displayed a high specific capacitance of 1224.5 F g-1 at 1 Ag-1 [62].

A few stacked Ti3C2Tx nanosheets with a width of 2 nm and outstanding electrochemical performance were chosen as the -ve electrode material. Ultra-fine MoO2 nanoparticles with diameters of 5-10 nm were developed as the +ve electrode material. After vacuum filtration on cellulose paper, MXene and MXene-MoO2 dispersions were laser cut into microelectrodes. After the microelectrodes were moved to PET substrates, the completed in-plane AMSCs were dubbed MXene/MXene-MoO2-AMSCs

1.3 Motivation of Thesis

- With increase in demand of electrical energy day by day it also necessary to make electrical energy storage devices supercapacitors more and more efficient
- To minimize the cost for storing more energy in less area
- All portable device manufacturing companies are focusing to ensure the maximum storage of energy

- The world needs better materials for supercapacitors for storage electric energy for devices that are easily carried (small sized), long lasting and can make us consume less energy sources that are non-renewable
- Energy storage component like supercapacitors are backbone of different electric appliances.

1.4 Research Problem

Highly conductive material and of high energy density that may be a nanocomposite of different materials for the application of supercapacitor in order to get following results:

- To increase capacitance from 200 – 250 Fg^{-1} from MXene
- To increase energy density (From 15 $Whkg^{-1}$)
- To increase power density (From 10 kW kg^{-1})

1.5 Research Gap

- Capacitance of pure MXene based supercapacitors are not enough to meet industry demands which is greater than 300 F/g for pure MXene.
- Low energy density **(<15Whkg^{-1})** of supercapacitors needs to increase for better efficiency
- Electric devices based on supercapacitors also under consideration to make them better and better in terms of efficiency, size, cost and electrical properties
- The Power density (10k W/kg) for the supercapacitors (SC) can be increased with new supposed Nano composite
- Supercapacitors based on individually for MXene and C60 already reported but supercapacitors based on composite of both MXene and Fullerene never used before

1.6 Thesis Objectives

- Synthesis of pure MXene from MAX (Commercially available)
- Synthesis of different nanocomposite materials (C60 + MXene) at optimized parameters
- To identify structural properties of samples (XRD)
- Investigation of morphology of nanocomposites of samples (SEM)
- Compositional analysis of various samples using EDX technique
- Identification of different RAMAN modes in series of samples

- Cyclic voltammetry (CV) to measure capacitance of samples
- To measure capacitance of all samples.

Chapter 02

2. FABRICATION AND CHARACTERIZATION

2.1 Etching of MXene from MAX

2.1.1 Etching Process

Etching is a technique used in nanofabrication to physically remove layers from a sample's surface. Etching is a process module that is quite significant. A "masking" substance that resists etching is used in various etch processes to shield a portion of the sample from the etchant.

2.1.2 Steps for Etching Process

Step 1

The HF/H2O2 combination was made by mixing 45 mL of HF with 5 mL of H2O2 in a 250 mL polypropylene bottle shown in Figure 2-1. Before adding 3g of Ti3SiC2 powder over the time span of 5 minutes, this etchant solution was continuously stirred in an ice bath (5 ^{0}C) for 20 mins.

Figure 2-1: Mixing of chemical precursors

Step 2

The plastic bottle was placed to an oil bath that had been pre-heated to 40 0C after 2 hours of constant stirring at 55^{0} C, and the reaction was allowed to continue for 45 hours with non-stop stirring (500rpm using 2cm-longTeflon magnetic stirring bar) is shown in Figure 2-2.

Figure 2-2: Mixing of chemicals by Magnetic Stirring

Step 3

Centrifugation at 5000 rpm was used to repeatedly wash the Ti3C2 MXene acidic solution with deionized water (DI H2O) to neutralize the pH. Centrifuge 5804 is used during this process shown in Figure 2-3.

Figure 2-3: Centrifuge 5804

Step 4

After neutralizing the sample there is need of filtration. To do so vacuum filter setup will be used as shown in Figure 2-4.

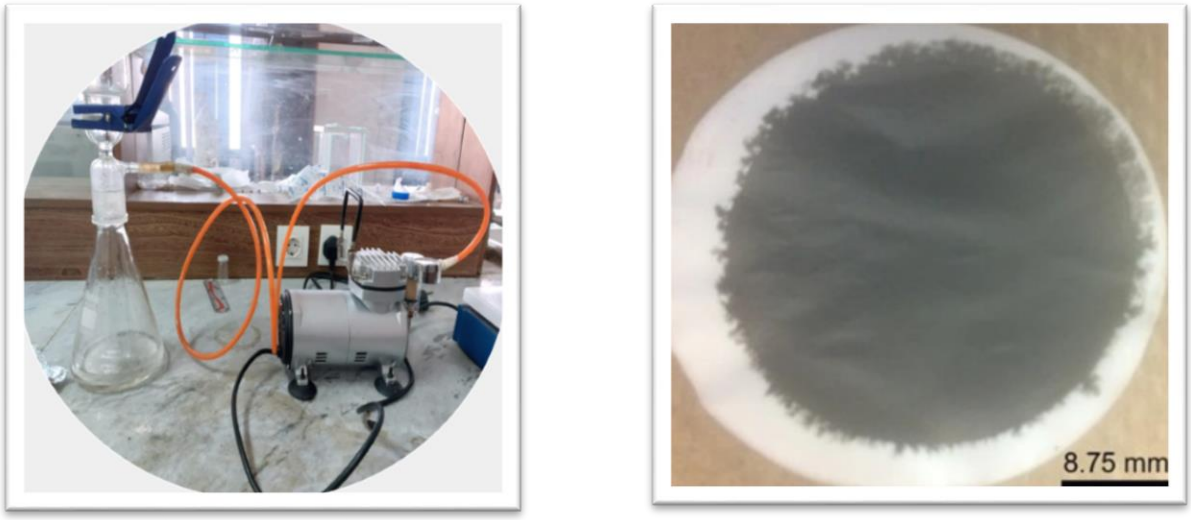

Figure 2-4: MXene without delamination after vacuum filtration

Step 5

MXene obtained from previous steps is need to be delaminate. Delamination is the process in which we increase the gap between the layers of MXene. To do so we add TMAOH (Tetramethyleammonium Hydroxide) with magnetic stirrer and put the sample on hot plate at 55^0C for 24 Hours shown in Figure 2-5.

Figure 2-5: Stirring at Hot Plate of MXene

Step 6

After adding TMAOH we have to normalize the ph of sample. To do so we place the sample in centrifuge machine at 5000 rpm for 8 min. we will repeat this process again and again and will

check the pH of sample after each washing. Washing will continue until ph of sample will become normal.

Step 7

After neutralizing the sample there is need of filtration. To do so, vacuum filter setup will be used. We will get final 2D delaminated sheets of MXene (Ti_3C_2).

2.2 Hydrothermal Process

One of the most popular ways to prepare nanomaterials is by hydrothermal production. Fundamentally, it requires a solution-reaction-based process. Nanomaterials would be designed by hydrothermal production over extensive series of temperatures, from very low to extremely high.

2.2.1 Mechanism of Hydrothermal process

There are following steps to make nanocomposite of MXene and C60 with hydrothermal process.

Step 1:

C60 is available commercially in powder form. MXene obtained from MAX is also in powder form. First step is to disperse both MXene and C60 in suitable solvents to covert the state of materials from powder into liquid form. Suitable solvents for MXene is DI Water and for C60 is dilute Ethanol.

To do dispersion we mix 20mg of MXene in 20mL of DI Water in a beaker and 20mg of C60 with 20mL of ethanol in another beaker. After mixing both materials in their suitable solvents, leave both beakers in sonication bath for about 30 Min shown in Figure 2-6.

During sonication materials will get sound energy form sonication bath and easily disperse inside the solvents.

Figure 2-6: Sonication of MXene and C60

Step 2:

After sonication both MXene and C60 are converted into disperse state. Then mix dispersive state of both MXene and C60 into Teflon beaker. This Teflon beaker then placed inside the autoclave and kept in oven at 90^0C for 24 Hours Shown in Figure 2-7.

During this process materials will get high temperature and pressure which is the basics of hydrothermal process and mix with each properly.

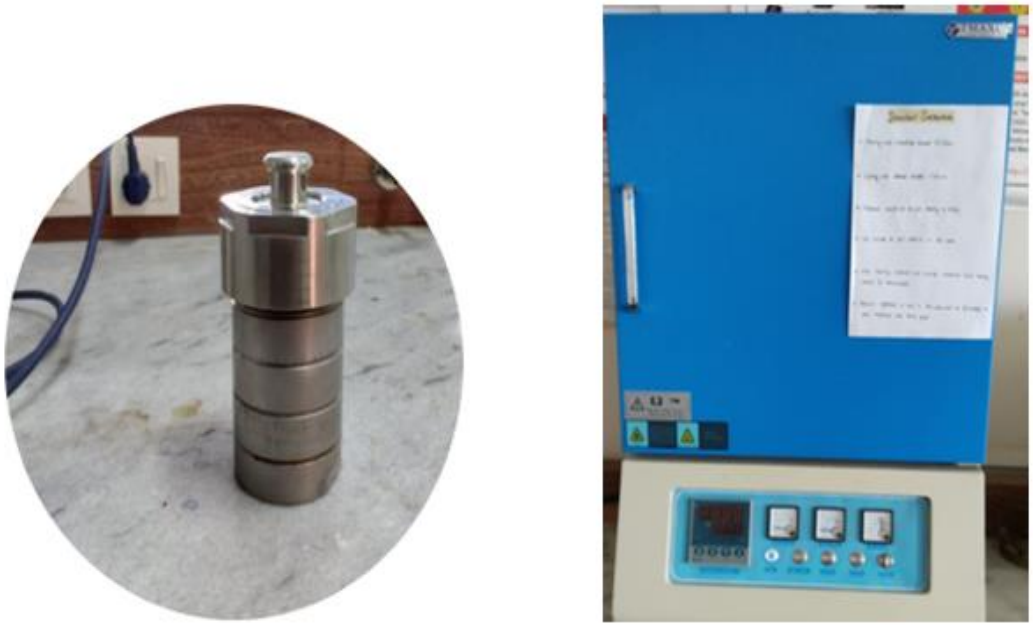

Figure 2-7: Heating and Mixing of MXene and C60

Step 3:

After 24 Hours of heating the mixture of both materials at high temperature and high pressure, now it's time to remove it from heater. After removing from heater the sample is kept in room temperature for 30 min to decrees the temperature of sample from 90^0C to room temperature.

Step 4:

To separate the solvents from material we use vacuum filtration with filter paper of 0.22 um pore size to get powder form of the composite of both MXene and C60.

Step 5:

After vacuum filtration we will get nanocomposite but this sample still have some amount of solvents like DI Water and ethanol in some amount in it. To dry it completely we kept the filter paper upon which we already obtained our nanocomposite inside the vacuum drying chamber at 100^0C for 24 hours.

Step 6:

After 24 hours we will get pure nanocomposite of both MXene and C60 which we will use further to determine its different characteristics like CV curves, XRD, SEM / EDX and RAMAN.

2.3 Fabrication of Electrode for Supercapacitors

The method used in electrode manufacturing is crucial in determining supercapacitor performance. The production phases, including as mixing, casting, spreading, and solvent evaporation conditions, all affect the final attributes of the electrode. These procedures have an impact on the final characteristics of Supercapacitors electrodes.

2.3.1 Types of Substrates used of making electrodes

Most commonly used substrates for making electrodes are as under:

- Nickel Foams
- FTOs (Fluorine doped tin oxides)
- Cobalt Foams

2.3.2 Mechanism of Electrode's Fabrication

Here we use Nickel foam as substrate for making electrode using nanocomposite of MXene and C60.

Step 1:

Firstly, we will wash nickel foam substrate to remove all impurities from it. For efficient washing, this process could be done twice. First, we will put nickel foam in such amount of Ethanol in a beaker as it completely dipped inside the ethanol. We will place nickel foam inside ethanol, in sonication bath for about 10 min. After we repeat same process in sonication bath again for 10 min but this this time with DI water. After this we will dry nickel foam on hot plate at 55^0C until it completely dry out as shown in Figure 2-8.

Figure 2-8: Drying of Nickle foam

Step 2:

After washing if substrates we will make slurry paste of active material. Here's active material will be nanocomposite of MXene and C60.

To make 100% slurry paste we will mix 80% of active material, 10% Carbon Black (C.B), 10% PVDF polyvinylidene difluoride (which is highly non-reactive thermoplastic flouropolymer) and 2 drops of NMP (N-Methyl-2-pyrrolidone).

With above composition we will use 2mg of active material, 0.2 mg of C.B, 0.2 mg of PVDF and 2 drops of NMP a small beaker. Mix these all components for slurry paste in a small beaker and place beaker in sonication bath for 10 min.

Step 3:

Once all essential components of slurry paste got mixed, we will spread this paste onto the nickel foam uniformly all over the surface with help of spray gun and kept nickel foam inside vacuum drying at 100^0C for 24 hours shown in Figure 2-9.

Figure 2-9: Dispersion of material over Nickel foam

Step 4:

After drying of electrode, we will wrap this into an aluminium foil to keep it safe from environmental impurities. Then it's time to compress the electrode at 5 psi pressure under hydraulic press machine as shown in Figure 2-10. This will distribute all components of slurry paste onto nickel foam uniformly and we will get final electrode to use it further finding IV curves for cyclic voltammetry.

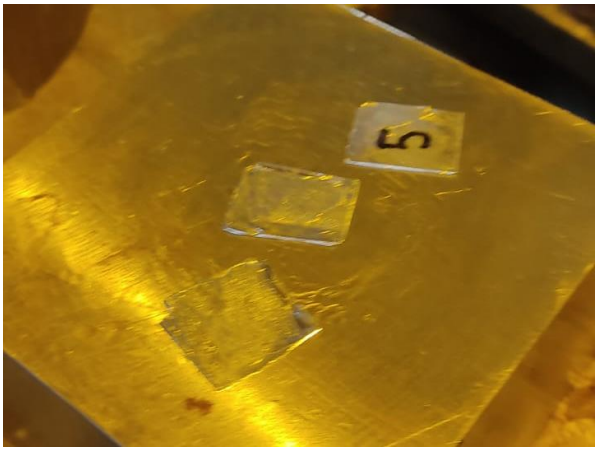

Figure 2-10: Electrodes after compressing

2.4 List of Required Chemicals

Following are materials used in synthesis process.

- MAX (Ti_3AlC_2)
- C60
- DI Water
- Ethanol
- Filter Paper
- Nickel Foam
- Carbon Black
- PVDF
- NMP
- Potassium Hydroxide
- Hydrofluoric Acid
- Hydrogen Per Oxide
- TMAOH

2.5 Characterizations

2.5.1 XRD Spectroscopy

2.5.1.1 Principle

X-ray diffraction's fundamental principle is the constructive interference of monochromatic X-rays with a crystalline material. The X-rays are generated by a cathode ray tube, which is then filtered to create monochromatic radiation, collimated, and directed towards the sample.

It served as an X-ray wave length three-dimensional diffraction grating. In those days, XRD was the method most commonly utilized for material characterization.

German scientist Mas von Laue made the discovery of crystalline material behavior, or the spacing of planes in a crystal lattice, in 1912.

2.5.1.2 Purpose of XRD

By employing X-rays, X-ray diffraction (XRD) assists in determining a molecule's geometry or structure. Long-range order exists in the phenomena of elastic scattering of X-rays from material atoms.

2.5.1.3 Type of equipment used

- Electron microscopes and similar equipment used for materials research
- X-ray diffraction equipment
- A high-voltage x-ray irradiator
- Cabinet x-ray systems
- Radiography equipment used for x-raying artwork
- Medical x-ray systems
- X-ray fluorescence analyzers (portable and bench-top)
- X-ray photoelectron spectrometers
- Electron beam evaporators
- Neutron generators

2.5.1.4 Working

A crystalline material's component cell proportions and phase classification may be determined quickly and logically using this approach. Since the X ray wavelength is in the 1–100 nm range, it is an excellent instrument for examining the structure of nanomaterials.

This approach makes it simple to learn about a material's crystal structure, the kind of phase it contains, the lattice parameter, and grain size [63, 64]. The XRD method is suitable for various types of materials, including powder, bulk, and thin films. Using this approach, it is simple to learn a material's crystallinity, the kind of phase it contains, the lattice parameter, and the grain size [9, 10]. All types of materials, including powder, bulk, and thin films, may be analysed using the XRD method. Mathematical expression of Bragg's law as under:

$$2d\sin\theta = n\lambda \qquad \textit{Equation 2-1}$$

Here d= inter planer spacing

θ= Bragg's angle as shown in Figure 2-11.

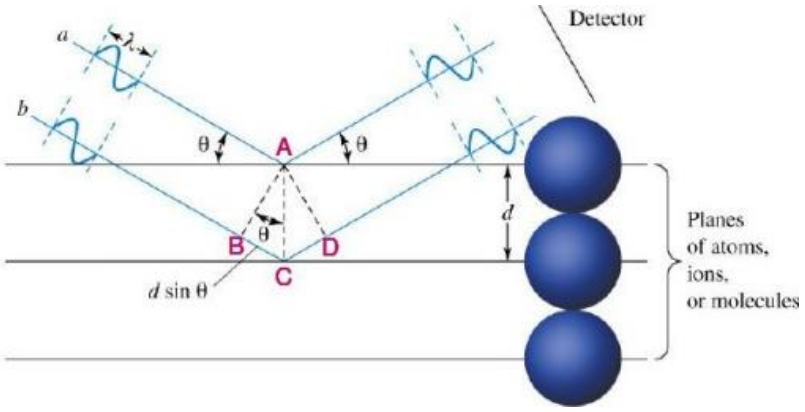

Figure 2-11: Principle of Bragg's Law

The diffracted X-rays are then found by scanning the crystalline material at a variety of 2 angles. All potential diffraction of the lattice must be realized because of the powdered material's placement being random. By translating diffraction peaks to d-spacing, it is possible to recognize each material since it has a unique set of d-spacing. Peak broadening may be used to determine the size of the nanomaterial. If the Nano crystalline size is smaller than, it may be estimated using the Scherrer equation.

$$\boldsymbol{D = \frac{k\lambda}{\beta cos\theta}} \qquad \textit{Equation 2-2}$$

D = Average crystallite size

λ = X-ray wavelength (0.9A)

β = Full width at half maximum [65].

2.5.2 SEM (Scanning Electron Microscope)

In a SEM, a focused electron beam is used to scan the surface of a sample, producing images of the material. The signals produced by the electrons' contacts with the sample's atoms disclose the sample's surface morphology and chemical makeup.

2.5.2.1 Type of equipment used in SEM

Essential components of all SEMs include the following:

- Electron Source ("Gun")
- Electron Lenses
- Sample Stage
- Detectors for all signals of interest
- Display / Data output devices
- Infrastructure Requirements:

- Infrastructure Requirements:
  - Power Supply
  - Vacuum System
  - Cooling system
  - Vibration-free floor
  - Room free of ambient magnetic and electric fields

2.5.2.2 Working

A concentrated beam of high-energy electrons is employed by SEM to produce different signals on the surface of solid objects. The signals that are acquired from the electron sample interactions provide information on the material that makes up the sample, including material alignment, crystalline assembly exterior morphology, and chemical composition.

The majority of applications collect data on the material's surface above a certain region to produce a two-dimensional picture that illustrates the spatial variation of these attributes [66]. The scanning mode of this method, which can photograph areas with spatial resolutions of between 50 and 100 nm and magnifications ranging from 20 to 30,000 times, is a benefit.

Thermionic released electron beam with tungsten filament is used in SEM and is produced by an electron cannon. The focus of a high energy electron beam is a limited area. As soon as this beam touches a sample's surface, electrons start to lose energy due to scattering and absorption. By exchanging energy, electrons and the sample form electromagnetic radiations by reflecting and emitting electrons. These reflected and released electrons and emitted radiations are detected with the use of detectors to create a magnified image. Backscattered electrons are best used to show differences in composition in multiphase samples, whereas these electrons are most useful for showing morphology and topography on materials. Inelastic collision is the source of X-ray production. Working principle of SEM is shown in Figure 2-12.

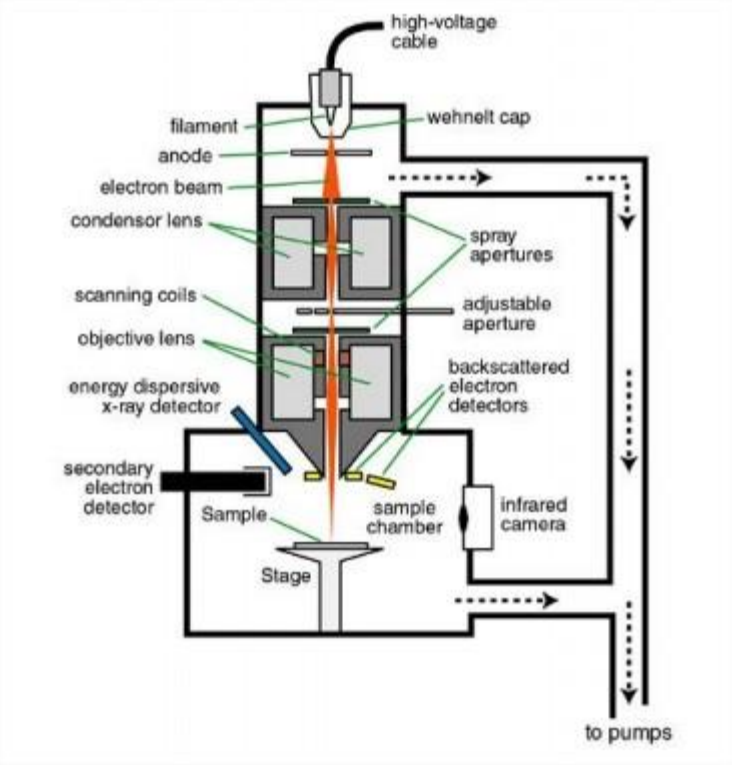

Figure 2-12: Working principle of SEM

2.5.3 EDX (Energy Dispersive Spectroscopy)

The analytical technique of energy dispersive X-ray spectroscopy (EDX) is used to characterize materials analytically or chemically. In general, EDX systems are coupled to an electron microscope, such as a transmission electron microscope (TEM) or a scanning electron microscope (SEM) (SEM). The foundation of EDX is the emission of a specimen's distinctive X-rays.

2.5.3.1 Principle of EDX spectroscopy

The fundamental idea behind EDAX is the creation of X-rays from a sample using an electron beam. The features and type of the elements contained in the sample are used to create the X-rays. Therefore, this method may also be used to determine how much energy X-rays are emitting.

2.5.3.2 Working

Bremsstrahlung X-rays and characteristic X-rays are the two types of X-rays produced as a result of these interactions. The X-rays are detected using an energy dispersive detector, which displays the signal as a histogram with a spectrum of intensity and x-ray energy. While the intensities of the properties of X-rays allow for the quantification of the element concentrations, the

characteristic X-ray energies recognize the sample by allowing elements. The energy of the beam typically ranges between 10 and 20 keV [66].

When an electron stream from a radioactive substance strikes the surface of a conducting material, X-rays are created. The sample being studied affects the X-ray energy emission. In a region with a depth of about 2 microns, the X-ray is produced. Every sample's component may be seen in two dimensions by moving the electron beam through the material. It is challenging for EDX to detect components with low atomic numbers. A detector known as the lithium drifted silicon detector is frequently used by EDX. It must operate in temperatures close to liquid nitrogen.

Once an X-ray hits the detector, a photoelectron will be generated inside the detector's body. This photoelectron creates electron-hole pairs as it passes through. Strong electric fields aid in drawing holes and electrons to the detector's opposing sides. Therefore, the amount of created electron-hole pairs, which depend on the energy of the incoming X-ray, determines the magnitude of the current pulse that is produced. Therefore, presenting proof of the material's investigated elemental composition aids in obtaining the Xray spectrum. The EDX system beryllium window frequently shields the SiLi detector. Working Principle of EDX is same as SEM discussed above.

2.5.4 Raman Spectroscopy

Raman spectroscopy is a scientific technique that uses scattered light to determine the vibrational energy states of a substance. It is titled after Indian physicist C. V. Raman, who discovered Raman scattering with his research partner K. S. Krishnan in 1928. Raman spectroscopy can identify chemicals based on their unique Raman "fingerprint," as well as provide structural and chemical data. This information is collected by Raman spectroscopy, which searches for Raman scattering in the substance.

2.5.4.1 Raman Scattering

When a molecule scatters light, the photon's changing electromagnetic field causes the molecular electron cloud to polarise, transferring the photon's energy to the molecule and left it in a higher state of energy. This is frequently referred to as the molecule's virtual state and may be thought of as the formation of a very transient complex between among the photon and the molecule. The photon is immediately reemitted as diffused light because the imaginary state is unstable. Figure 2-13 depicts the RAMAN scattering process.

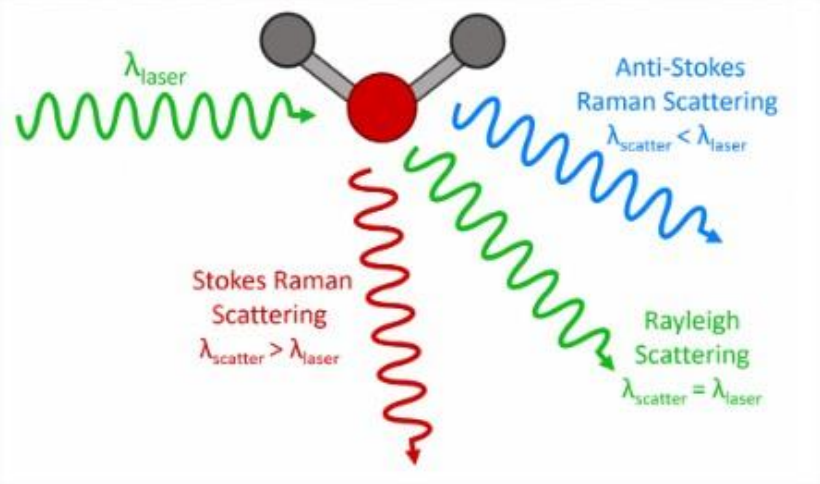

Figure 2-13: Three types of scattering processes that can occur when light interacts with a molecule.

From a quantum mechanical standpoint, both Stokes and Anti-Stokes processes are equally feasible. Because the Boltzmann distribution predicts that the majority of molecules in an ensemble would oscillate in the ground state, Stokes scatter is statistically the more likely process. As a result, in Raman spectroscopy, the Stokes Raman scattering is virtually always detected. Figure 2-14 shows that the Stokes Raman scatter has always been intense than the anti-Stokes scatter.

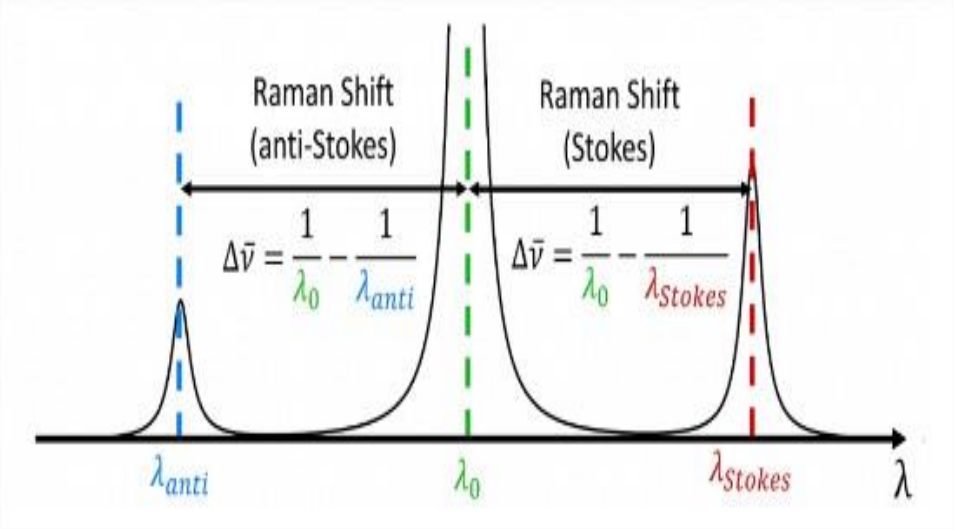

Figure 2-14: Diagram of Rayleigh, Stokes and Anti-Stokes Raman Scatter

2.5.5 Cyclic voltammetry (CV)

An electrochemical method for determining how much current a redox active solution responds to a linearly cyclic potential sweep between two or more pre-set values. It is a valuable technique for

quickly obtaining details on the redox process thermodynamics, the analytical energy levels, and the kinetics of electronic-transfer reactions.

Cyclic voltammetry uses a three-electrode system:

- Working Electrodes
- Reference Electrodes
- Counter Electrode

In order to perform cyclic voltammetry, an electrolyte solution, a baseline solution, and three electrodes are first introduced into an electrochemical cell. The potential among the working and reference electrodes is then swept linearly using a potential state until it reaches a specified limit, at which point it is reversed.

This technique is done numerous times during a scan, and the device continually detects the varying current between the working and counter probes. The result is a cyclic voltammogram, which has a characteristic duck-shaped plot.

An electrochemical cell's electrical potential can be measured potentiometrically in static situations (i.e. no current flow). The Nernst equation states that the standard potential for a generic reduction or oxidation (redox) reaction depends on the concentration of the reactants (A) and products (B) at the electrode/solution interface:

$$aA + ne^- \Leftrightarrow bB$$

$$E = E^{0\prime} - \frac{2.303RT}{nF} log \frac{[B]^b}{[A]^a}$$

Equation 2-3

Here, E stands for the electrode potential, E0′ for the formal potential, R stands for the gas constant (8.3145 J.K-1.mol-1), T stands for temperature, n stands for the quantity of electron moles involved, and F stands for the Faraday constant (96,485 C.mol-1).

The ratio of products to reactants, elevated to their respective stoichiometric powers, is denoted by the phrase [B]b/[A]a. When the concentration is low enough (0.1 mol.dm3), this can be substituted for an activity term.

The Nernst equation can be written as:

$$E = E^{0'} - \frac{0.0591}{n} log \frac{[B]^b}{[A]^a}$$

Equation 2-4

2.5.5.1 The Three Electrode System

While cyclic voltammetry (as well as other voltammetry methods) only require two electrodes in theory, maintaining a constant voltage and ensuring that its impedance measured is the one at the working electrode-solution contact can be difficult. Passing the needed current all while current that passes to neutralise the redox processes at the electrode surface might be difficult in both cases. As a consequence, the responsibility for reference the chosen for the following and regulating the current generated is usually distributed across three electrodes. Diagram of three electrode system is shown in Figure 2-15.

Figure 2-15: Three Electrode cell as used in cyclic voltammetry with an Ossila Potentiostat

The potential of the working electrode is changed while the potential of the reference electrode is held constant by an electrochemical redox reaction with a predetermined value in order to monitor and regulate the applied potential difference. The reference electrode, which is typically made of a silver wire and a saturated solution of silver ions, must have consistent amounts of each reaction component in order to maintain a steady voltage.

$$i_d = nFAD_0\left(\frac{\delta C_0}{\delta x}\right)_0$$

Equation 2-5

i_d = Diffusion-limited current,

A = Electrode area

D_0 = diffusion coefficient of the analyte

$(\partial C_0/\partial x)_0$ = Concentration gradient at the electrode surface.

2.5.5.2 Cyclic Voltammogram

The 'duck-shaped' plot generated by cyclic voltammetry is called a cyclic voltammogram. The scan begins at -0.4V in the example cyclic voltammogram and advances to progressively positive, oxidative potentials. At first, the voltage is insufficient to cause the analyte to oxidize.

The commencement of oxidation is achieved when the potential methods several kT of the normal potential, and while the analyte is being oxidized at the working electrode surface, the current exponentially rises (b). Here, the current rises first as if the concentration of the oxidant has not changed, which is typical for a reversible process. From this point on, the current is constrained by the sluggish (on the scale of electrochemistry) mass transfer of analyte from the bulk to the DDL interface. As the abilities are perused more positively, this causes the current (d) to drop until a constant is achieved where additional increases in potential have no further impact. When a scan is reversed to negative potentials (a reductive scan), the analyte is continuously oxidized until the applied potential reaches a point at which it may be reduced again (e). The reduction process is similar to the oxidation process, with the exception of the scan direction being the reverse and the cathode peak (ipc) occurring at the cathodic peak potential (Epc) (f).

Cyclic Voltammogram graph is shown in Figure 2-16.

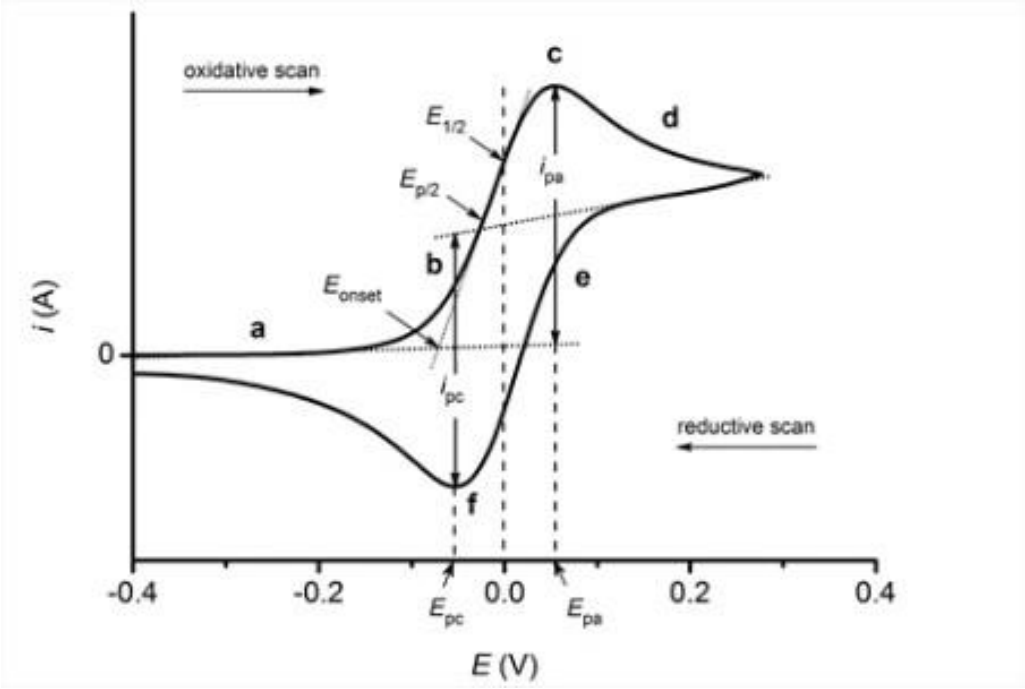

Figure 2-16: Cyclic Voltammogram graph

2.5.5.3 Electrochemical solutions

The electrochemical solution required for cyclic voltammetry typically comprises of different components as under:

- The compound of interest (10^{-3} – 10^{-5} M)
- An electrolyte (0.1 M)
- A solvent that dissolves the chemical of interest as well as the electrolyte.

Chapter 03

3. STRUCTURAL AND OPTICAL ANALYSIS

3.1 XRD Analysis

XRD graph for MAX (TI_3AlC_2) which is commercially available. We use MAX as a raw material for getting MXene (Ti_3C_2).

3.1.1 XRD Graph for Both MAX (Ti_3AlC_2) and MXene (Ti_3C_2)

The XRD graph for MAX (Ti_3AlC_2) and MXene (Ti_3C_2) with their peaks and corresponding planes are shown in Figure 3-1 below. Analysis of peaks are performed at software Jade and OriginPro is used for plotting the graph. MXene (Ti_3C_2) detected planes are (002), (004), (006), (008) and for MAX (Ti_3SiC_2) detected planes (002), (004), (006), (101), (103), (104), (008), (105), (108), (109), (110).

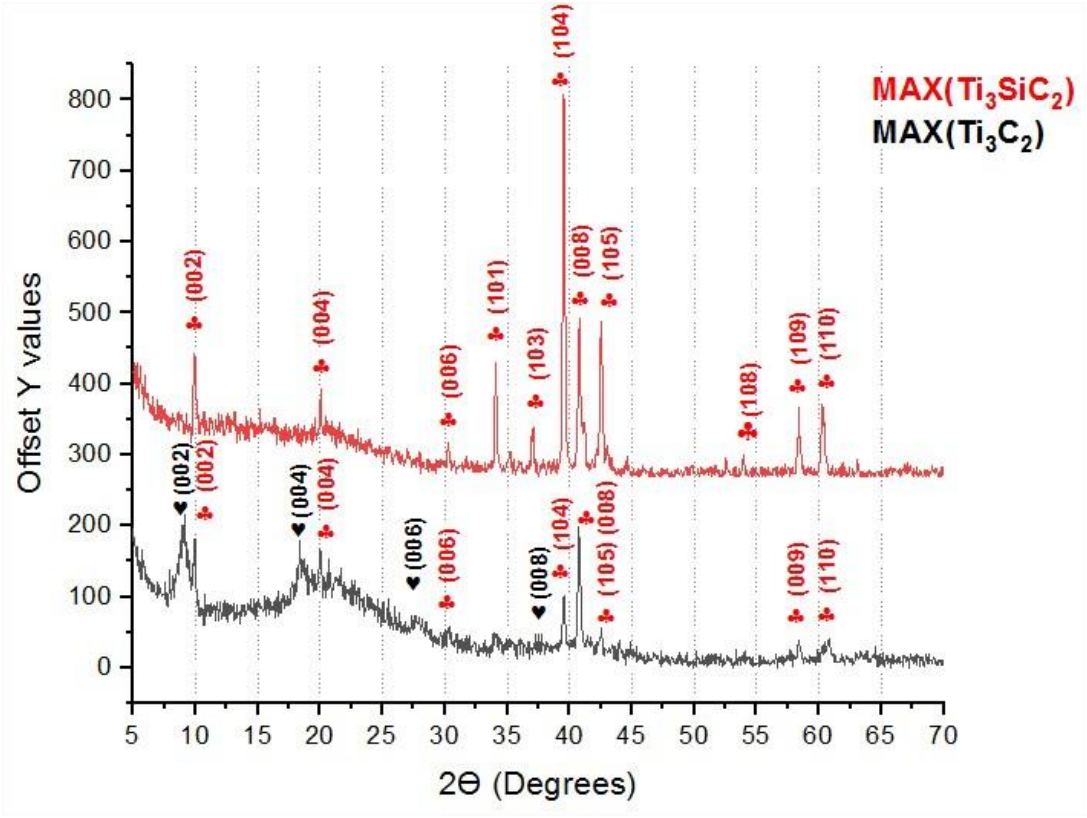

Figure 3-1: XRD Graph for MAX and MXene

Some mathematical calculation from XRD graph is shown in Table 3-1. Different formulas are used to calculate Crystallite Size, Micro strains and Dislocation Density by following formulas:

The average crystallite size determined by using Scherer formula:

$$\boldsymbol{D = \frac{0.9\lambda}{\beta cos\theta}} \qquad \textit{Equation 3-1}$$

Dislocation density calculated by formula:

$$\boldsymbol{\delta = \frac{1}{D^2}} \qquad \textit{Equation 3-2}$$

Micro strains calculated by formula:

$$\boldsymbol{\varepsilon = \frac{\beta cos\theta}{4}} \qquad \textit{Equation 3-3}$$

Table 3-1: Mathematical Calculations of XRD (MAX & MXene)

MAX(Ti_3SiC_2)		**MAX(Ti_3SiC_2)**	
Planes	(002), (004), (006), (008)	**Planes**	(002), (004), (006), (101), (103), (104), (008), (105), (108), (109), (110).
Crystal Size	88.9 nm	**Crystal Size**	84.13nm
FWHM	0.149	**FWHM**	0.125
D-Spacing	0.78956 nm	**D-Spacing**	0.43966
Micro Strain	0.035×10^{-6}	**Micro Strain**	0.045×10^{-6}

After successfully making MXene from MAX, 5 samples with different compositions. The samples with compositions are as under in Table 3-2

Table 3-2: Samples with Different Compositions of MXene and C60

Sample No	MXene Composition (%)	C60 Composition (%)
Sample 1	10%	90%
Sample 2	25%	75%
Sample 3	50%	50%
Sample 4	75%	25%
Sample 5	90%	10%

3.1.2 XRD result for MXene and C60 (Nano composite)

The composition of 1st Sample consists of 90 %(36mg) C60 + 10 %(4mg) MXene. The XRD graph of Sample 1 is shown in Figure 3-2 below. Planes of MXene detected are (006), (008), (110) for C60 (113), (222) and for MAX are (006), (101), (104), (105)

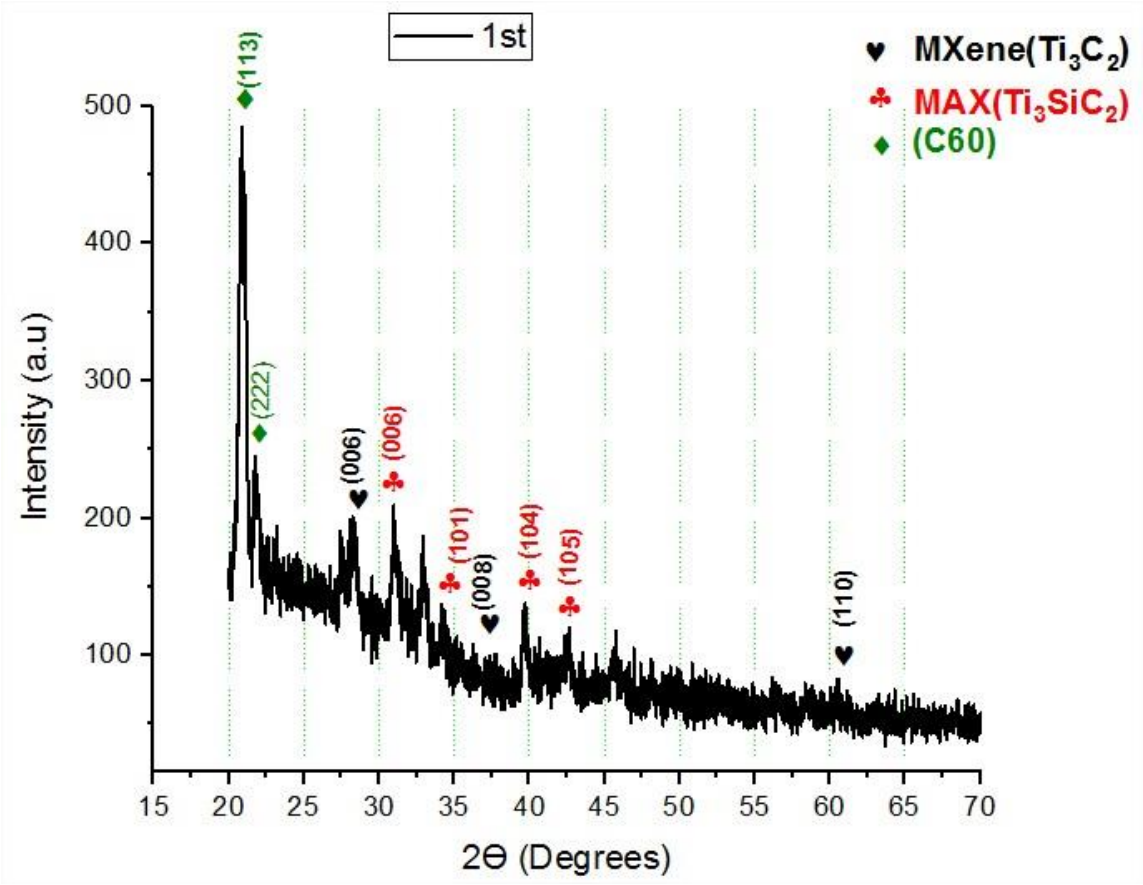

Figure3-2: XRD Graph of 90 %(36mg) C60 + 10 %(4mg) MXene

The composition of 3rd Sample consists of 50 %(20mg) C60 + 50 %(10mg) MXene. The XRD graph of Sample 3 is shown in Figure 3-3 below. Detected Planes of MXene are (002), (004), (006), (008), for MAX are (004), (006), (101), (104), (008) and for C60 are (111), (113), (222).

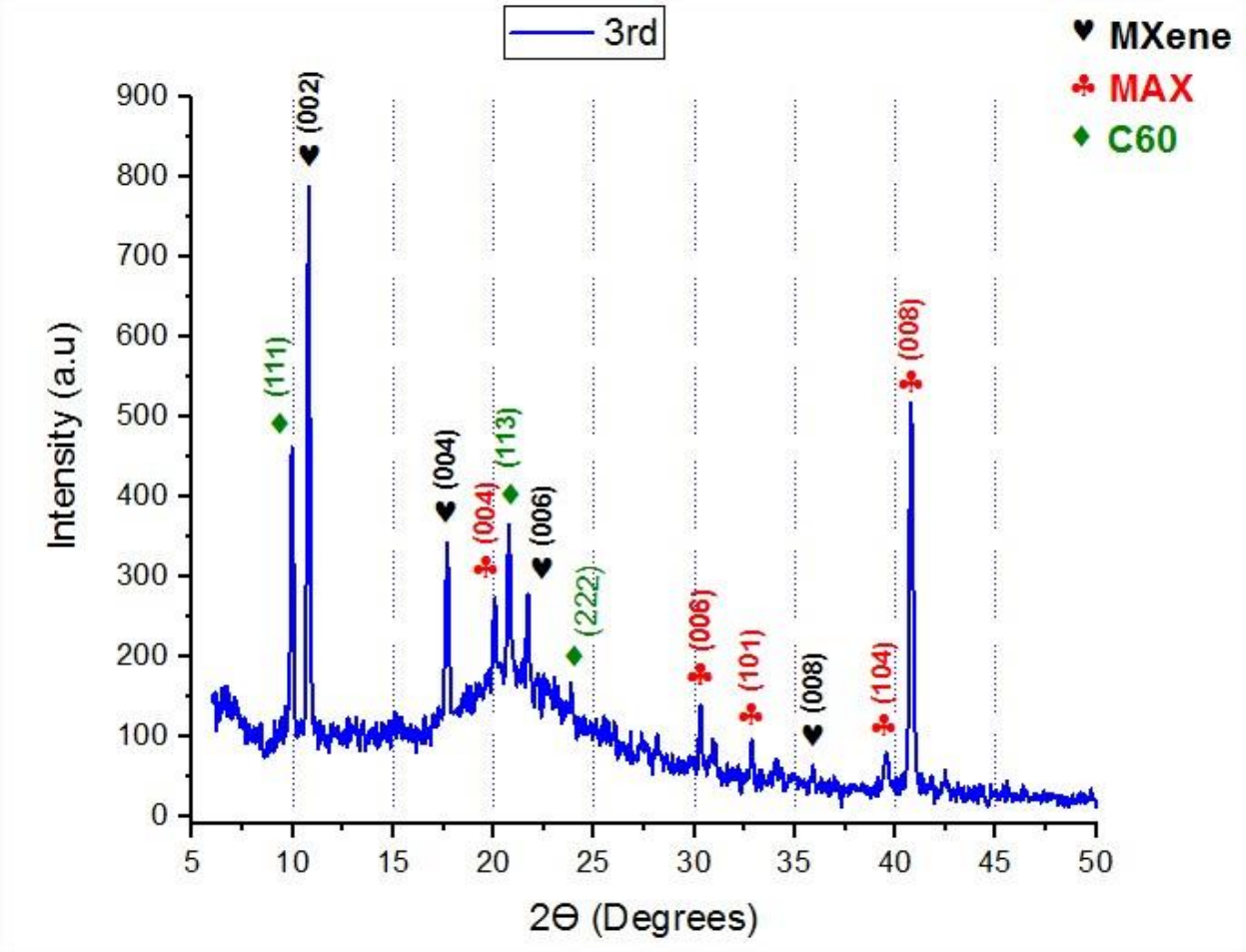

Figure 3-3: XRD Graph of 50 %(20mg) C60 + 50 %(10mg) MXene

Some mathematical calculation from XRD graph is shown in Table 3-3. Different formulas are used to calculate Crystallite Size, Micro strains and Dislocation Density by formulas of Equations 3-1 to Equation 3-3.

Table 3-3: Mathematical Calculations of XRD (Sample 3)

Structure(MXene)	Cubic
Planes	(002), (004), (006), (008)
Crystallite Size	62.9 nm
FWHM	0.129
D- spacing	0.81966 nm

Dislocation Density	2.53×10^{14} line/m^{2}
Micro Strain	0.055×10^{-6}

3.1.3 Combine XRD results of MAX, MXene, 1st sample and 3rd sample:

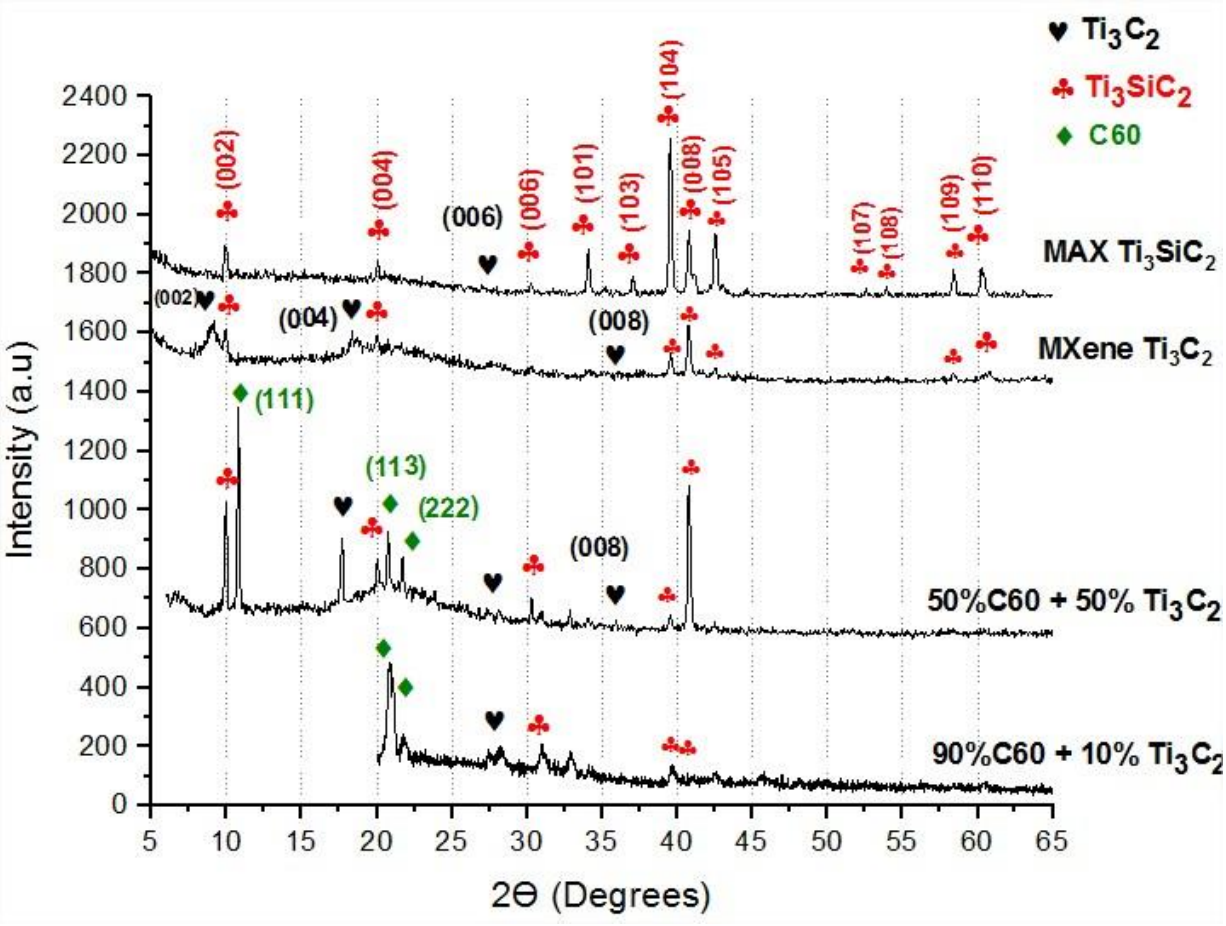

Figure 3-4: *Combine XRD results of MAX, MXene, 1st sample and 3rd sample:*

3.2 SEM and EDX Analysis

SEM and EDX is used to analyze the surface morphology and elemental composition of samples. Following Samples are characterized by SEM and EDX to analyze their properties.

3.2.1 C60/ Fullurene

The Figure 3-4 depicts the surface morphology of C60 structure at different resolutions. From surface analysis it is confirmed that C60 has Buckyball shape (sphere).

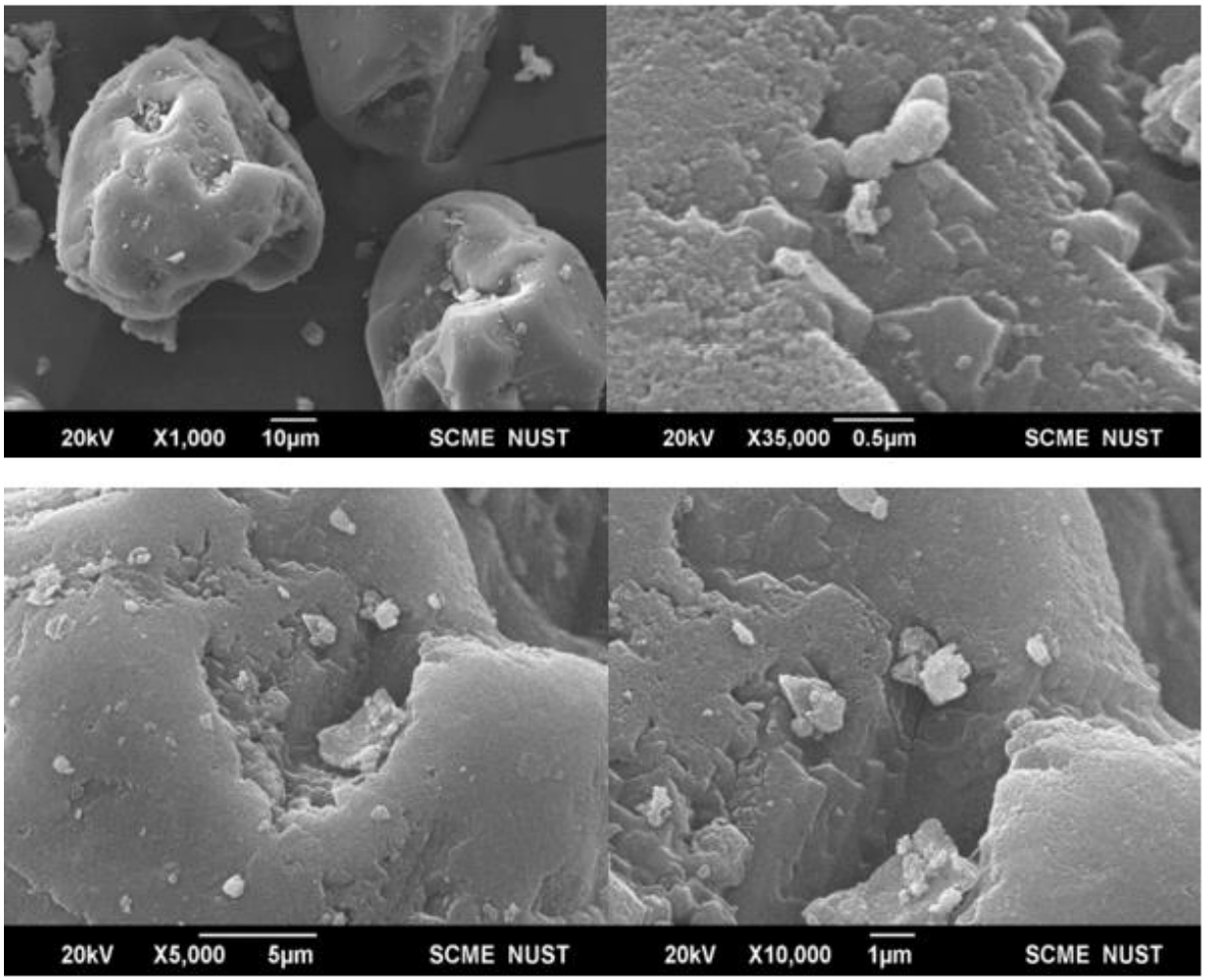

Figure 0-1: SEM Images of C60 Structure

3.1.1 EDX of C60

EDX analysis confirmed the elemental compositional ratio of samples C60. Figure 3-5 shows the ratio of elemental composition. The Intense peak of 100% ratio depicts that there is pure carbon present in sample which justifies the formation of Buckyball Structure.

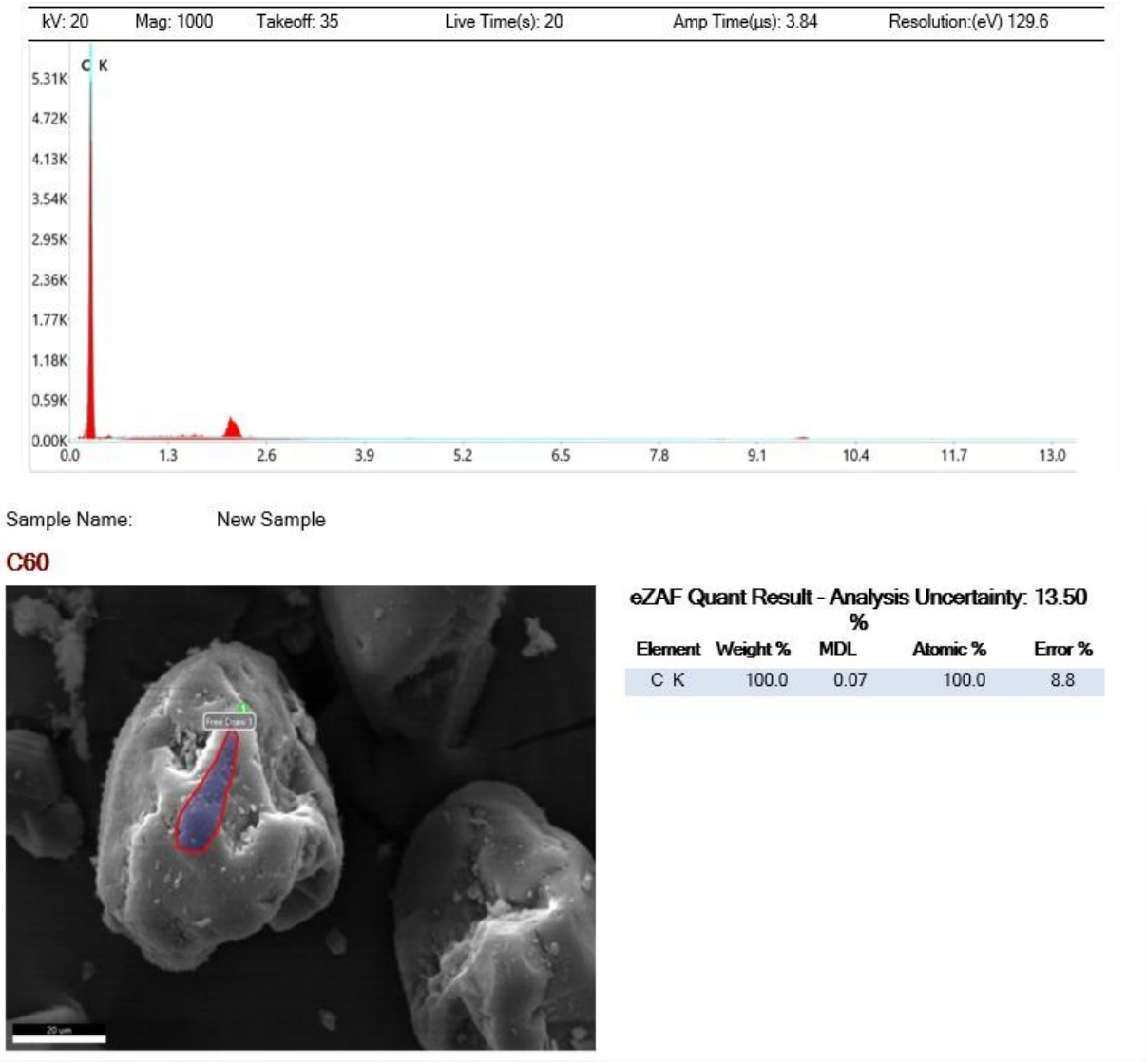

Figure 0-2: Elemental Compositional Ratio of Samples C60

3.1.2 SEM / EDX for 3rd Sample having 50%MXene and 50% C60 Composition

Figure 3-6 shows the surface morphology of Sample having 50% MXene and 50% C60 composition. In this structure it is revealed that MXene is scattered over the surface of Buckyball.

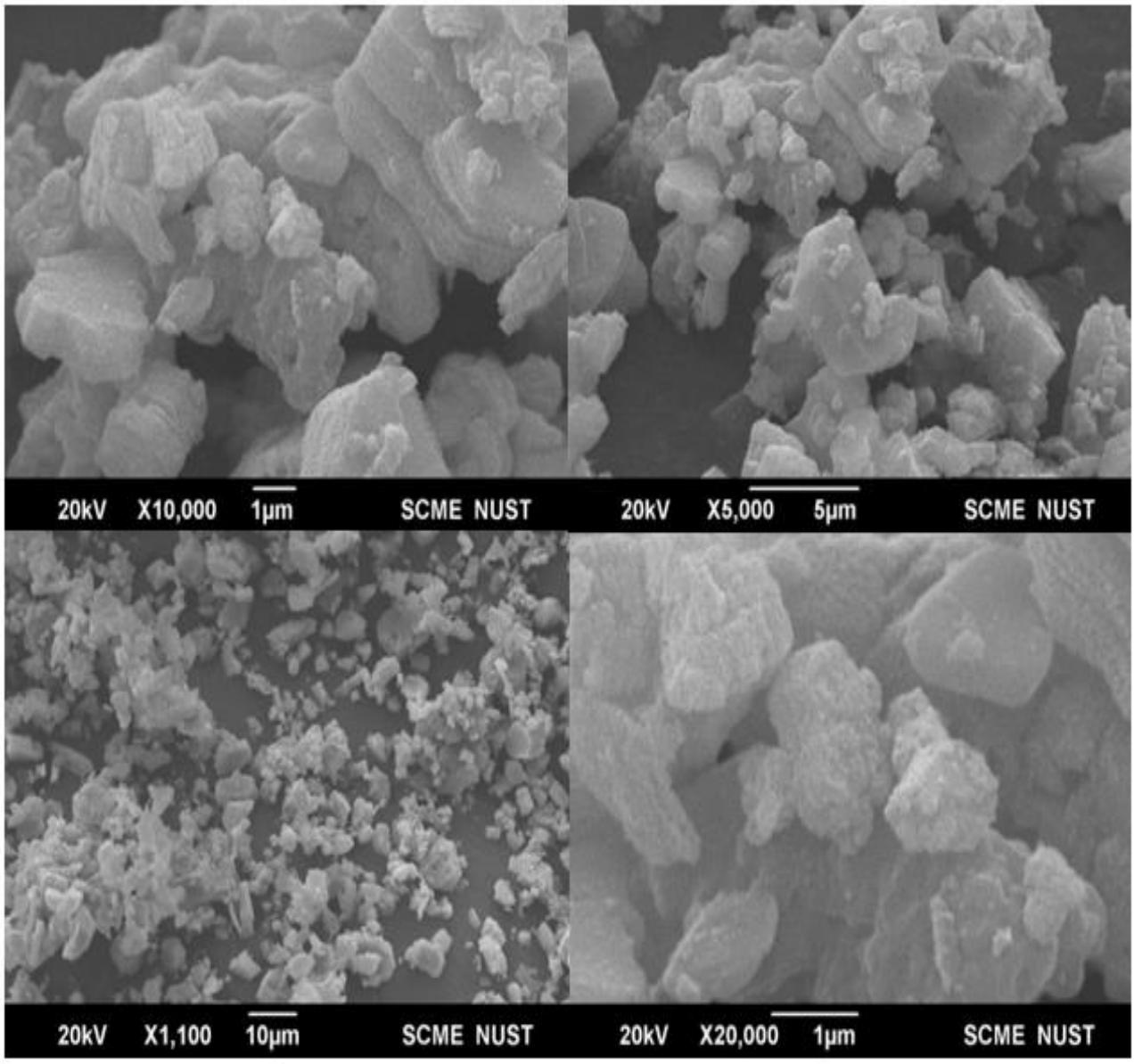

Figure 0-3: Surface Morphology of Sample having 50% MXene and 50% C60 Composition

3.1.3 SEM / EDX for 3rd Sample having 50%MXene and 50% C60 Composition

Figure 3-7 shows the elemental compositional ratio of Sample having 50% MXene and 50% C60 composition. From the graph it is revealed that different peaks of elements are detected by EDX spectroscopy consist of Titanium, Carbon and Silicon due to MAX while Fluorine and Oxygen peak is occurred because F and DI water is used during etching process. Nitrogen peak is also detected in this spectrum.

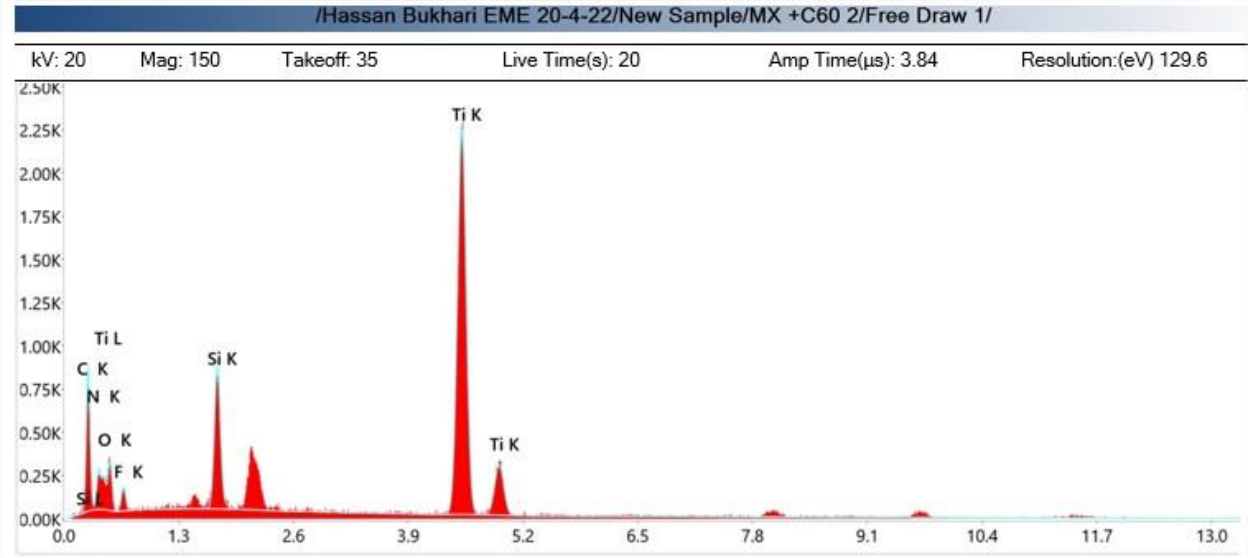

MX +C60 2

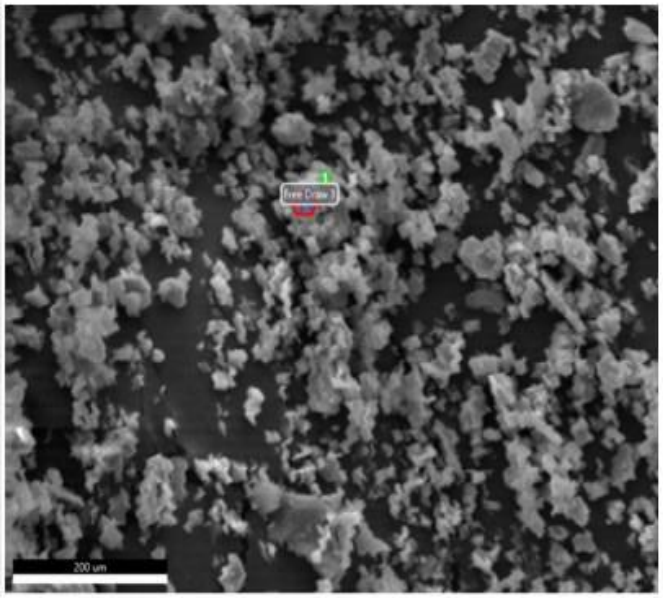

eZAF Quant Result - Analysis Uncertainty: 13.54 %

Element	Weight %	MDL	Atomic %	Error %
C K	27.4	0.64	46.9	11.9
N K	2.9	1.91	4.3	31.0
O K	15.9	1.50	20.5	15.3
F K	5.2	0.73	5.7	16.6
Si K	6.0	0.15	4.4	6.8
Ti K	42.5	0.27	18.3	2.4

Figure 0-4: Elemental Compositional Ratio of Sample having 50% MXene and 50% C60

3.2 RAMAN Spectroscopy

RAMAN spectroscopy is performed to analyze the vibrational modes of elements such as MAX, MXene and C60. All five samples show the peaks of MAX, MXene and C60 at different wavelengths. In all five samples Ti3C2, Ti3C2(OH)3 and Ti-C vibrational bonds detected. With increase in MXene concentration the peaks intensity of carbon bond is reduced and also the main vibration peaks of carbon disappeared. Figure 3-8 shows the graph of Raman shift and vibrational modes peaks.

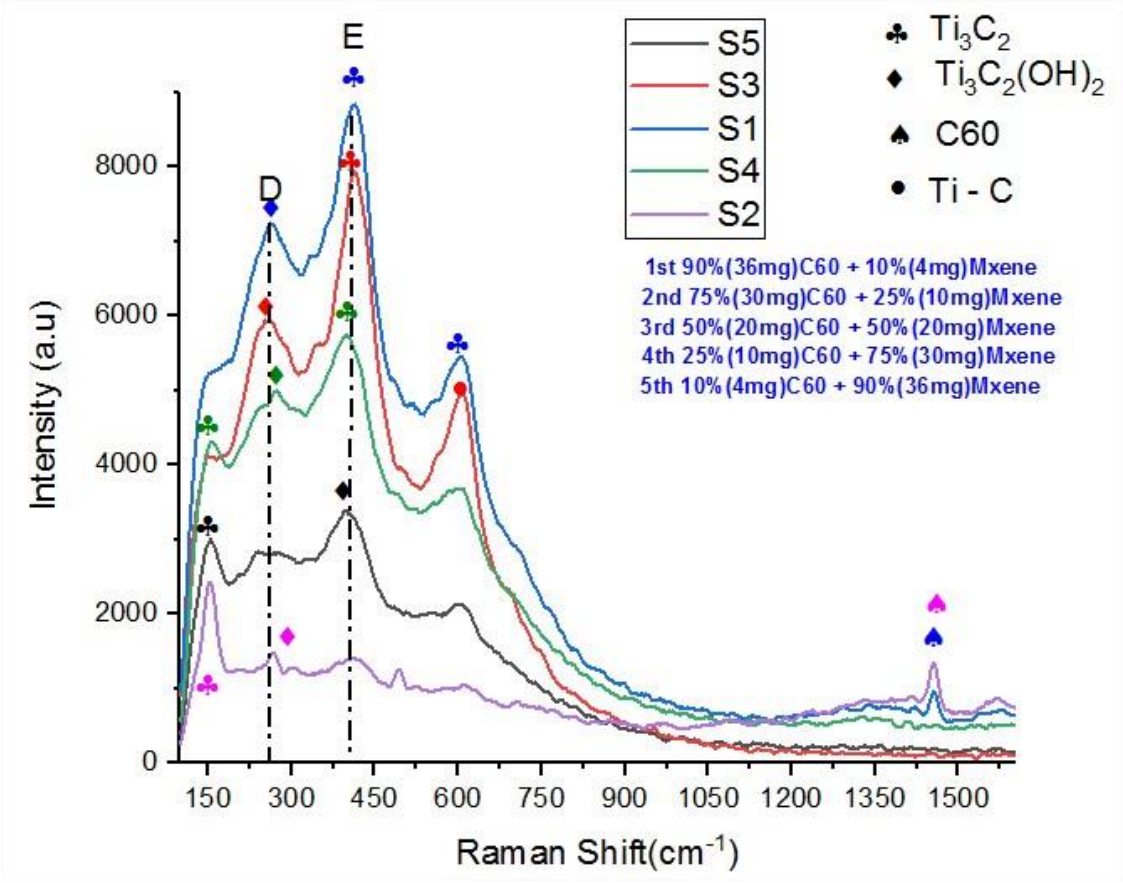

Figure 0-5: Graph of Raman Shift and Vibrational Modes Peaks

Chapter 04

4. Electrical Characteristics and Capacitances

In this chapter the electrical properties and capacitance of MXene, C60 and composites of MXene and C60.

4.1 Electrical properties (I-V curves) of each nanocomposite at various scan rates

I-V curves for 1st sample with composition of 90% (36mg) C60 + 10% (4mg) MXene at different scan rates shown in Figure 4-1. It shows that area of integration at 200 scan rate is maximum and for 2 scan rate its minimum. It means that oxidation and reduction at 200 scan rate is maximum.

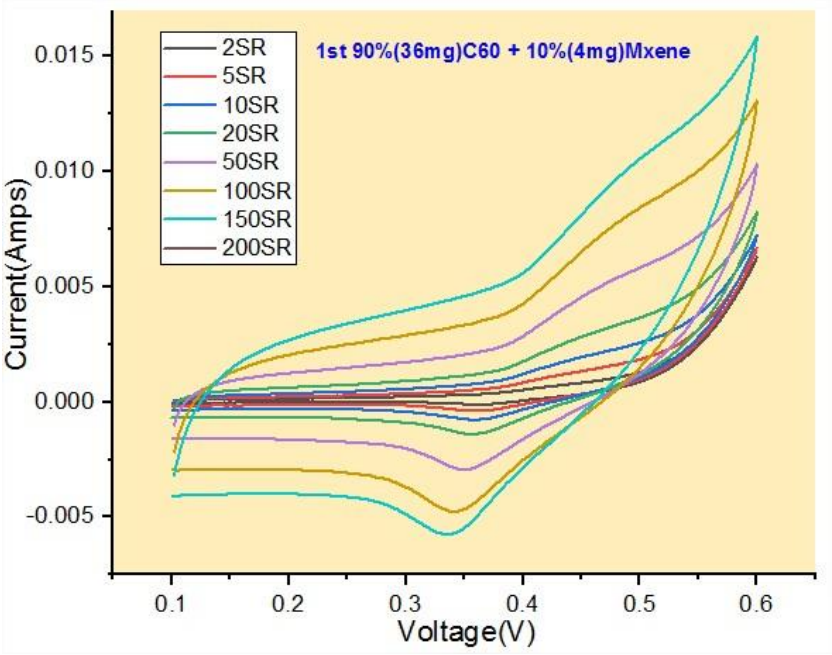

.Figure 4-1: I-V curves for 1st sample with composition of 90% (36mg) C60 + 10% (4mg) MXene at different scan rates

I-V curves for 2nd sample with composition of 75% (30mg) C60 + 25% (10mg) MXene at different scan rates is shown in Figure 4-2. It shows that area of integration at 200 scan rate is maximum and for 2 scan rate its minimum. It means that oxidation and reduction at 200 scan rate is maximum.

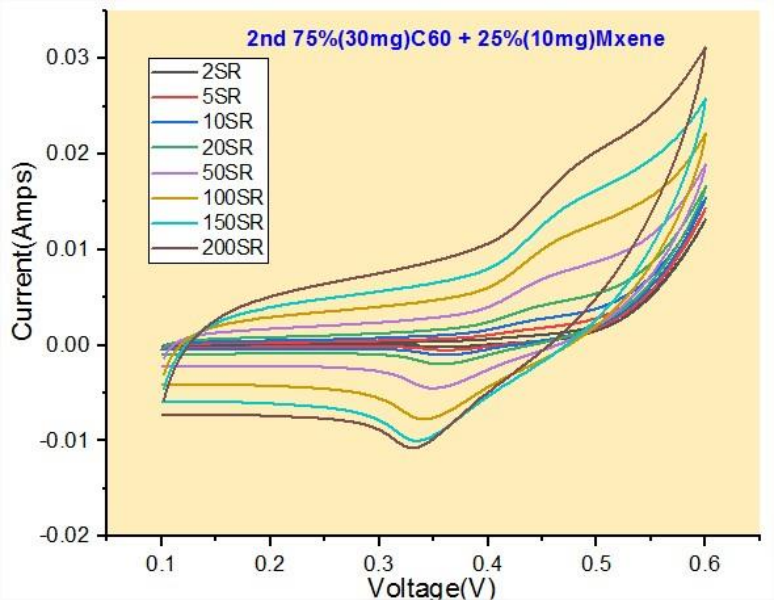

Figure 4-2: I-V curves for 2nd sample with composition of 75% (30mg) C60 + 25% (10mg) MXene at different scan rates

I-V curves for 3rd sample with composition of 50% (20mg) C60 + 50% (20mg) MXene at different scan rates is shown in Figure 4-3. It shows that area of integration at 200 scan rate is maximum and for 2 scan rate its minimum. It means that oxidation and reduction at 200 scan rate is maximum.

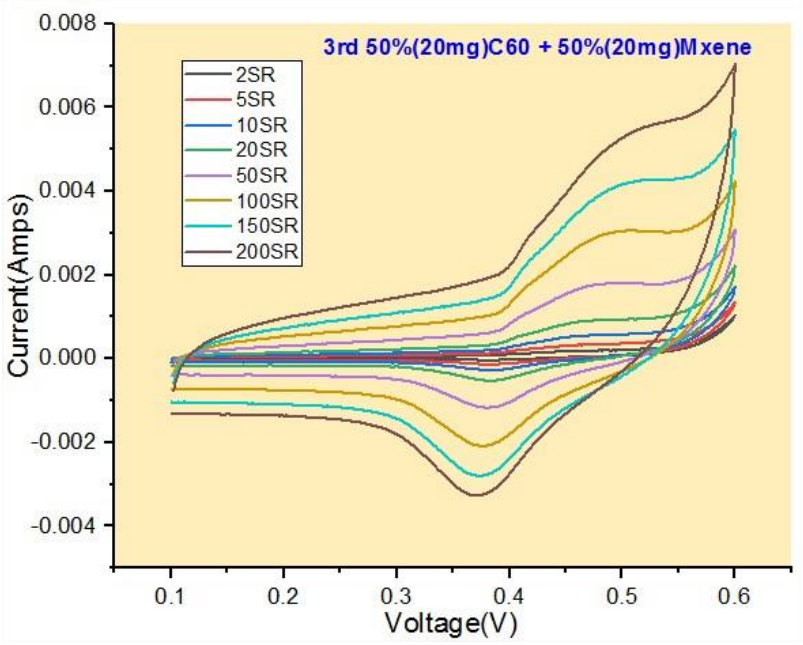

Figure 4-3: I-V curves for 3rd sample with composition of 50% (20mg) C60 + 50% (20mg) MXene at different scan rates

I-V curves for 4th sample with composition of 25% (10mg) C60 + 75% (30mg) MXene at different scan rates is shown in Figure 4-4. It shows that area of integration at 200 scan rate is maximum and for 2 scan rate its minimum. It means that oxidation and reduction at 200 scan rate is maximum.

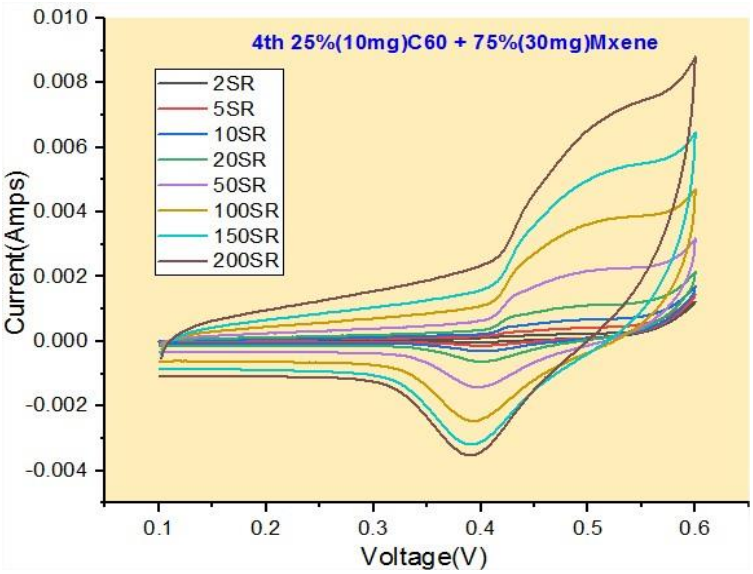

Figure 4-4: I-V curves for 4th sample with composition of 25% (10mg) C60 + 75% (30mg) MXene at different scan rates

I-V curves for 5th sample with composition of 10% (4mg) C60 + 90% (36mg) MXene at different scan rates is shown in Figure 4-5. It shows that area of integration at 200 scan rate is maximum and for 2 scan rate its minimum. It means that oxidation and reduction at 200 scan rate is maximum.

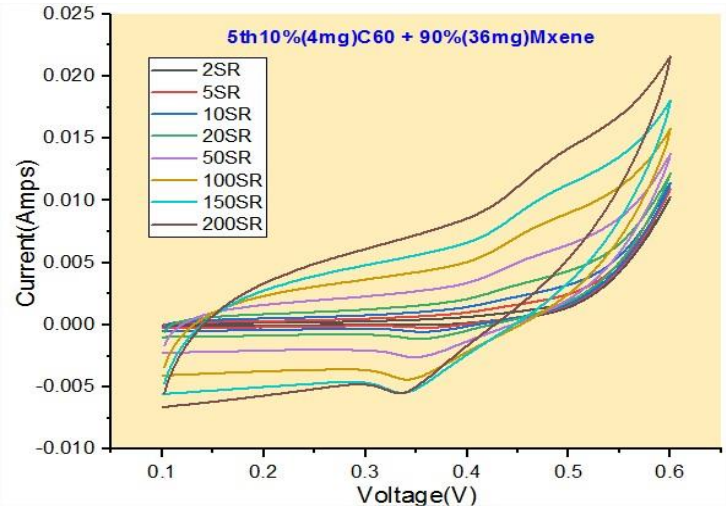

Figure 4-5: I-V curves for 5th sample with composition of 10% (4mg) C60 + 90% (36mg) MXene at different scan rates

4.2 Area of I-V Curves and Capacitances Vs Scan Rates

By using following equation 4-1, we will find capacitance of each sample at different scan rates with help of area under the curve.

$$C_s\ (F/g) = \frac{\int I\ dv\ (AV)}{m(g) \times SR(\frac{V}{s}) \times \Delta V(V)} \qquad \textit{Equation 4-1}$$

m: Active Mass (Constant) (1.5mg)

ΔV : Voltage Window (Constant) (0.5V)

This graph shows the behaviour that if capacitance have inverse relation with scan rates and area of integration have direct relation with scan rates for 1st sample shown in Figure 4-6.

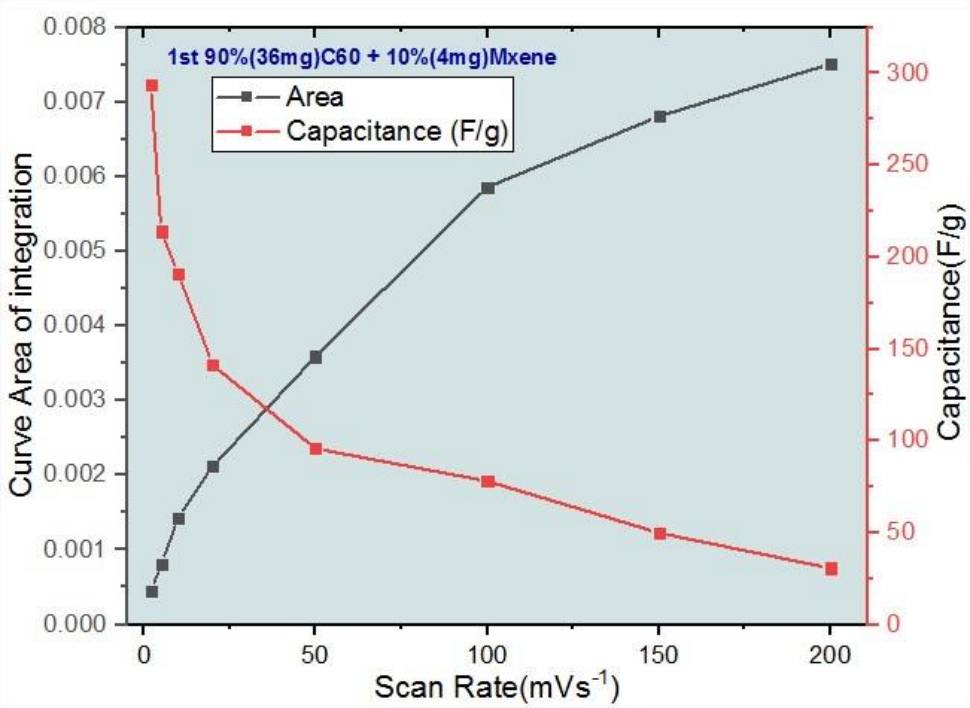

Figure 4-6: Capacitance and area of integration with scan rates for 1st sample

This graph shows the behaviour that if capacitance have inverse relation with scan rates and area of integration have direct relation with scan rates for 2nd sample shown in Figure 4-7.

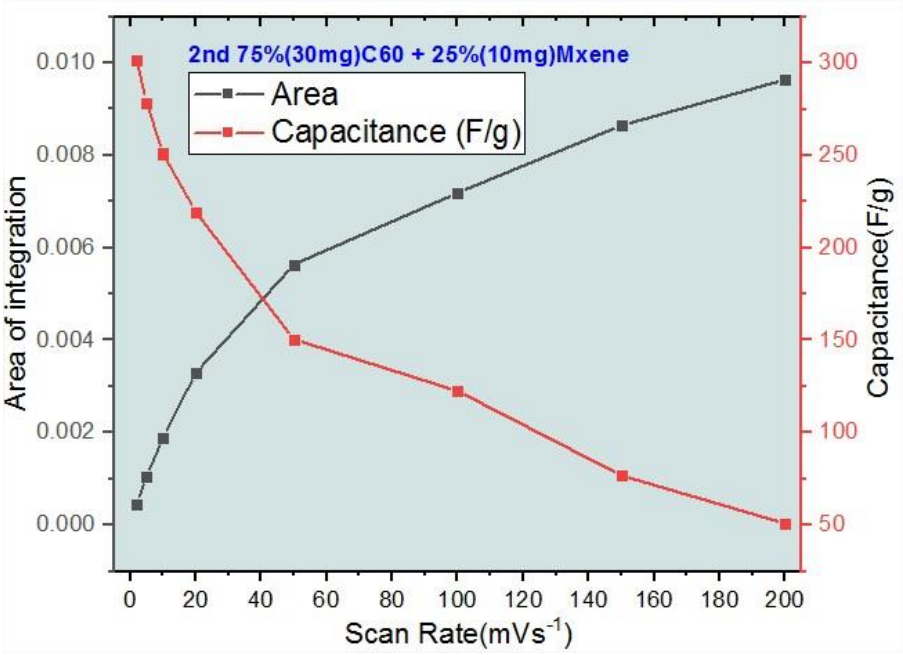

Figure 4-7:Capacitance and area of integration with scan rates for 2nd sample

This graph shows the behaviour that if capacitance have inverse relation with scan rates and area of integration have direct relation with scan rates for 3rd sample shown in Figure 4-8.

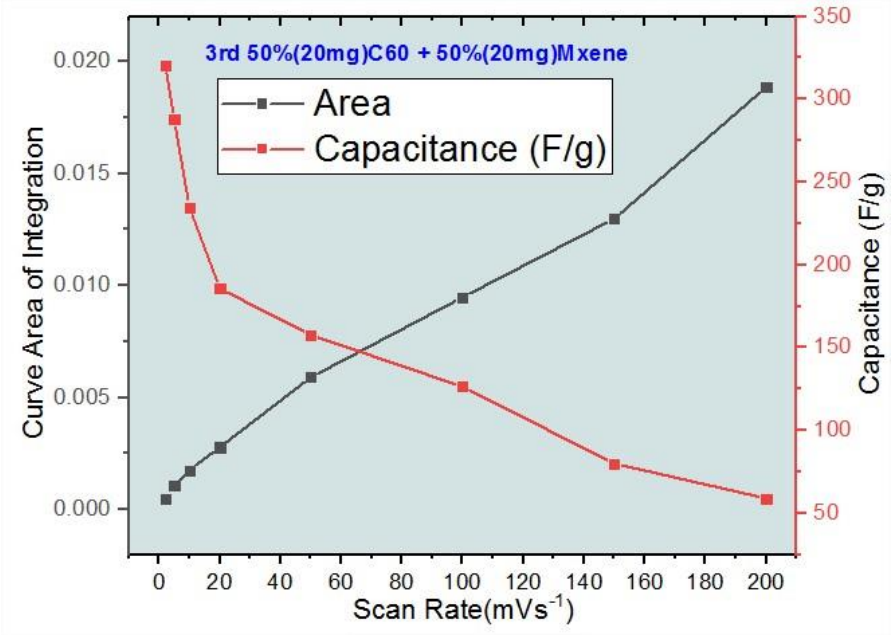

Figure 4-8: Capacitance and area of integration with scan rates for 3rd sample

This graph shows the behaviour that if capacitance have inverse relation with scan rates and area of integration have direct relation with scan rates for 4th sample shown in Figure 4-9.

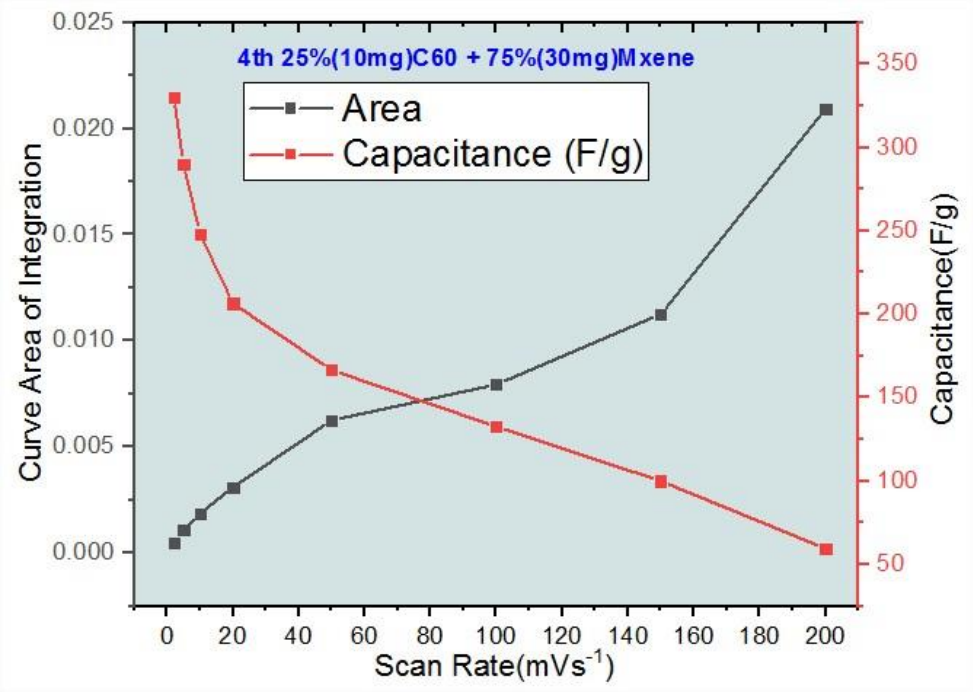

Figure 4-9: Capacitance and area of integration with scan rates for 4th sample

This graph shows the behaviour that if capacitance have inverse relation with scan rates and area of integration have direct relation with scan rates for 5th sample shown in Figure 4-10.

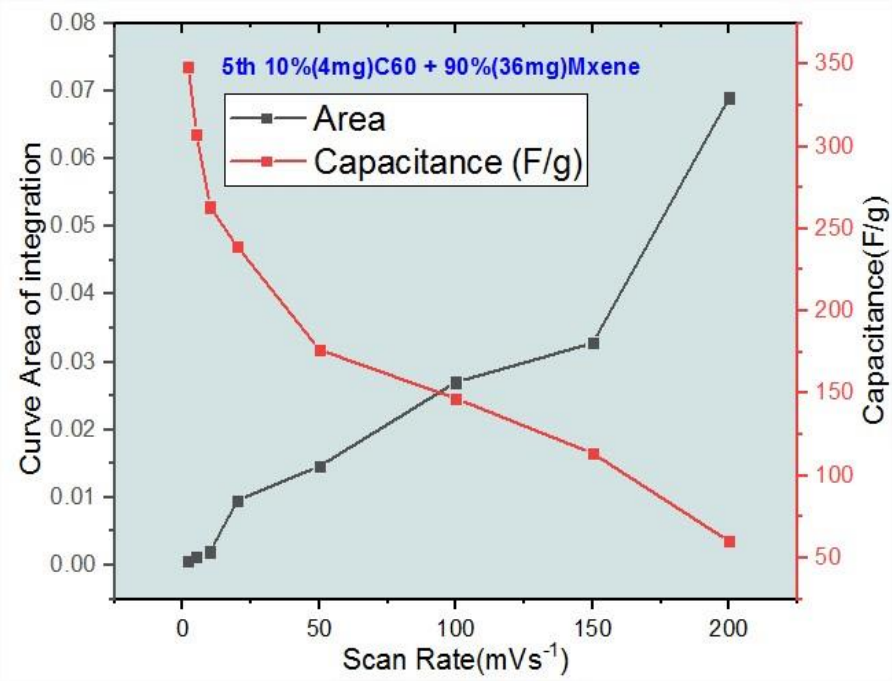

Figure 4-10:Capacitance and area of integration with scan rates for 5th sample

4.3 Current Vs Voltage Measurements for Cyclic Voltammetry for all samples at same Scan Rates:

I-V curves for all samples 1st, 2nd, 3rd, 4th, and 5th, at 2 Scan rate:

It shows that area of integration for 5th sample maximum and for 1st sample is minimum. It means that oxidation and reduction of 5th sample is maximum shown in Figure 4-11.

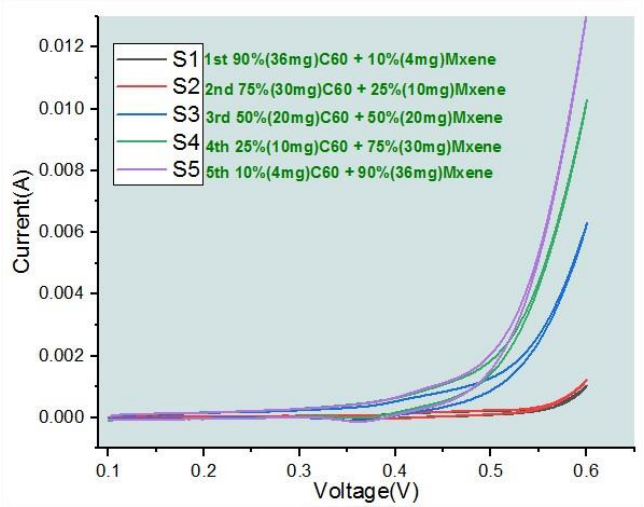

Figure 4-11: I-V curves for all samples 1st, 2nd, 3rd, 4th, and 5th, at 2 Scan rate

I-V curves for all samples 1st, 2nd, 3rd, 4th, and 5th, at 5 Scan rate:

It shows that area of integration for 5th sample maximum and for 1st sample is minimum. It means that oxidation and reduction of 5th sample is maximum as shown in Figure 4-12.

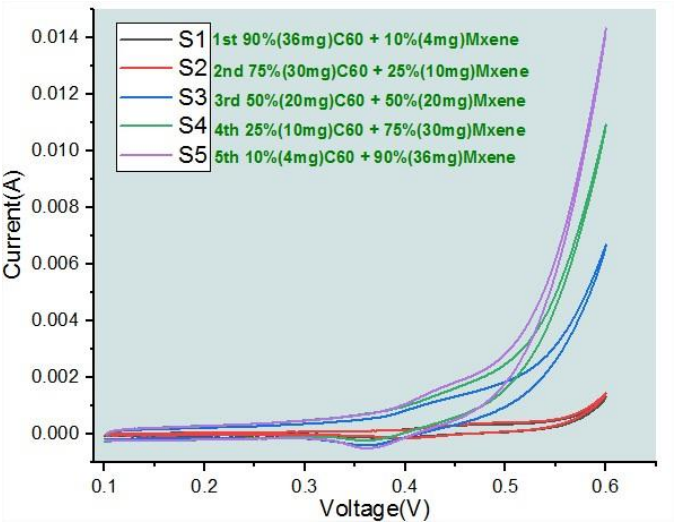

Figure 4-12: I-V curves for all samples 1st, 2nd, 3rd, 4th, and 5th, at 5 Scan rate

I-V curves for all samples 1st, 2nd, 3rd, 4th, and 5th, at 10 Scan rate:

It shows that area of integration for 5th sample maximum and for 1st sample is minimum. It means that oxidation and reduction of 5th sample is maximum as shown in Figure 4-13.

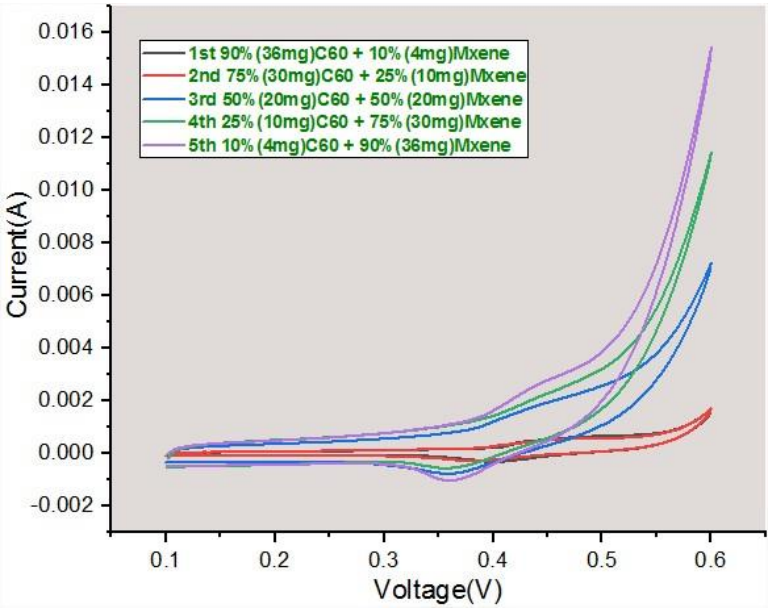

Figure 4-13: I-V curves for all samples 1st, 2nd, 3rd, 4th, and 5th, at 10 Scan rate

I-V curves for all samples 1st, 2nd, 3rd, 4th, and 5th, at 20 Scan rate:

It shows that area of integration for 5th sample maximum and for 1st sample is minimum. It means that oxidation and reduction of 5th sample is maximum as shown in Figure 4-14.

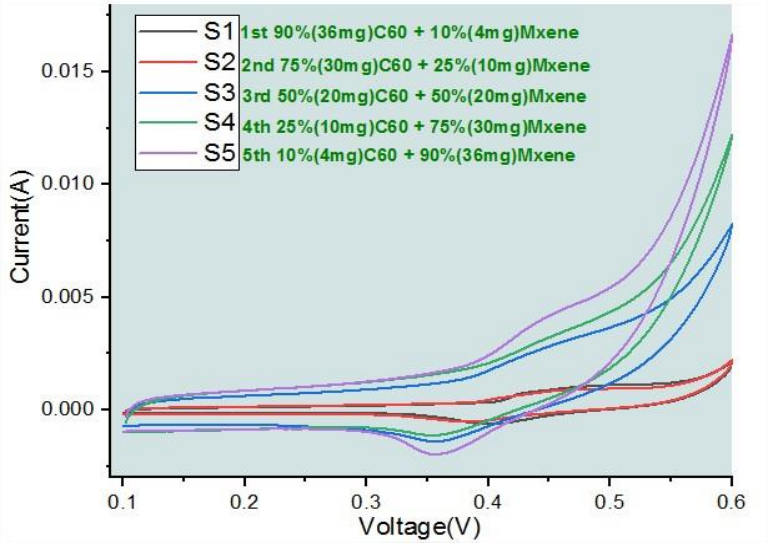

Figure 4-14: I-V curves for all samples 1st, 2nd, 3rd, 4th, and 5th, at 20 Scan rate

I-V curves for all samples 1st, 2nd, 3rd, 4th, and 5th, at 50 Scan rate:

It shows that area of integration for 5th sample maximum and for 1st sample is minimum. It means that oxidation and reduction of 5th sample is maximum as shown in Figure 4-15.

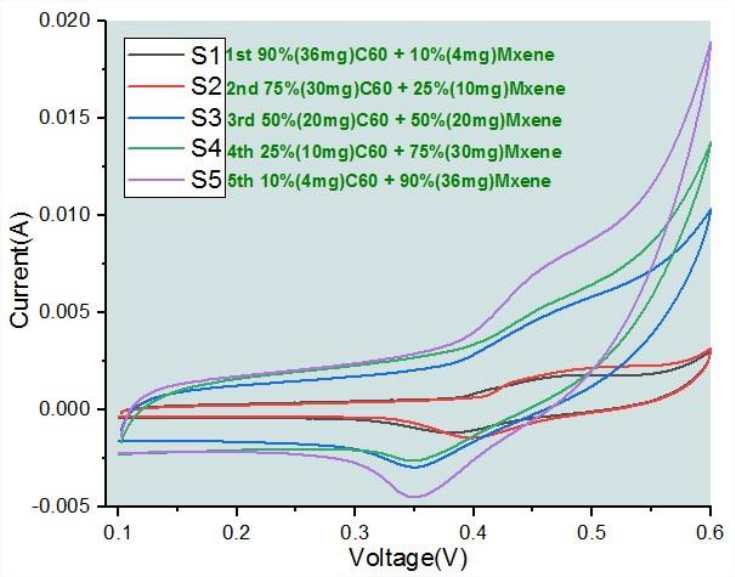

Figure 4-15: I-V curves for all samples 1st, 2nd, 3rd, 4th, and 5th, at 50 Scan rate

I-V curves for all samples 1st, 2nd, 3rd, 4th, and 5th, at 100 Scan rate:

It shows that area of integration for 5th sample maximum and for 1st sample is minimum. It means that oxidation and reduction of 5th sample is maximum as shown in Figure 4-16.

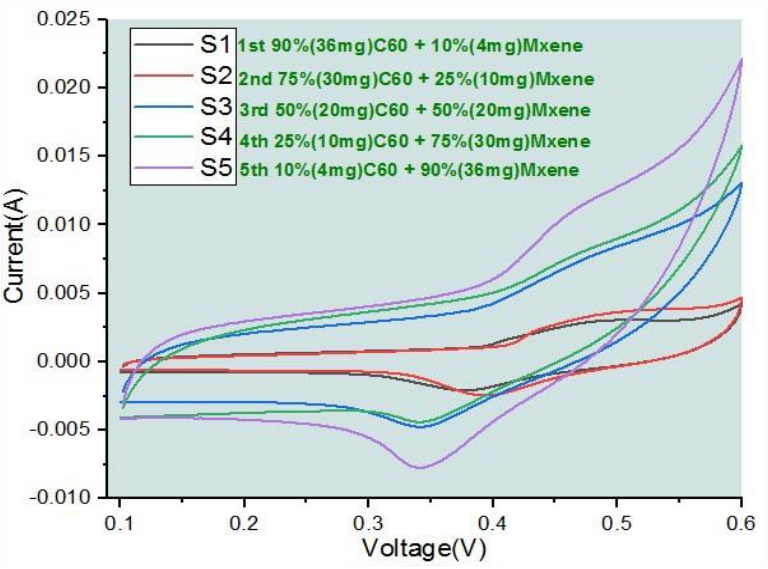

Figure 4-16: I-V curves for all samples 1st, 2nd, 3rd, 4th, and 5th, at 100 Scan rate

I-V curves for all samples 1st, 2nd, 3rd, 4th, and 5th, at 150 Scan rate:

It shows that area of integration for 5th sample maximum and for 1st sample is minimum. It means that oxidation and reduction of 5th sample is maximum as shown in Figure 4-17.

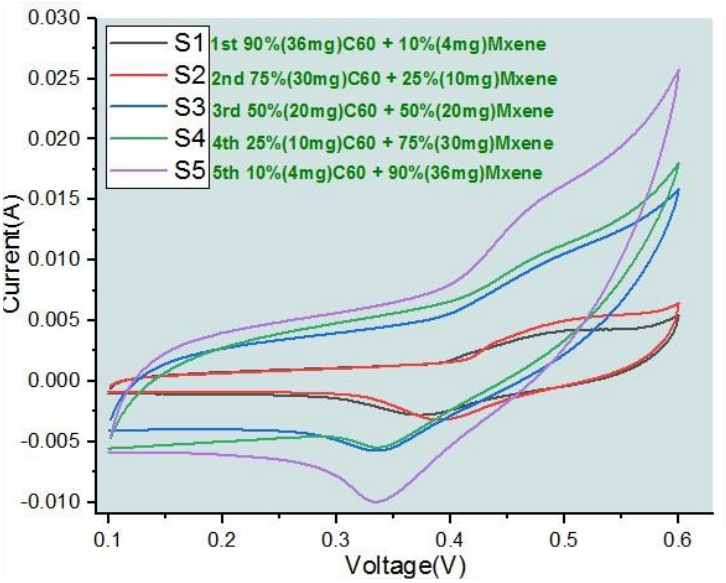

Figure 4-17: I-V curves for all samples 1st, 2nd, 3rd, 4th, and 5th, at 150 Scan rate

I-V curves for all samples 1st, 2nd, 3rd, 4th, and 5th, at 200 Scan rate:

It shows that area of integration for 5th sample maximum and for 1st sample is minimum. It means that oxidation and reduction of 5th sample is maximum as shown in Figure 4-18.

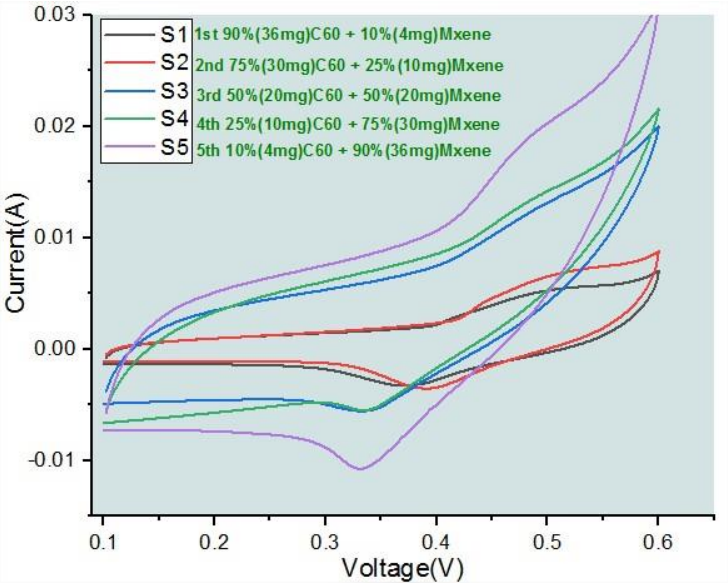

Figure 4-18: I-V curves for all samples 1st, 2nd, 3rd, 4th, and 5th, at 200 Scan rate

4.4 Capacitance of All compositions of nanomaterials at different Scan Rates:

This graph gives capacitance of each sample at different scan rates. This graph shows that with increase in composition of MXene the capacitance will also increase as shown in Figure 4-19. Here best suitable sample for better capacitance is 5th sample having maximum composition of MXene and it shows 348 Fg^{-1}.

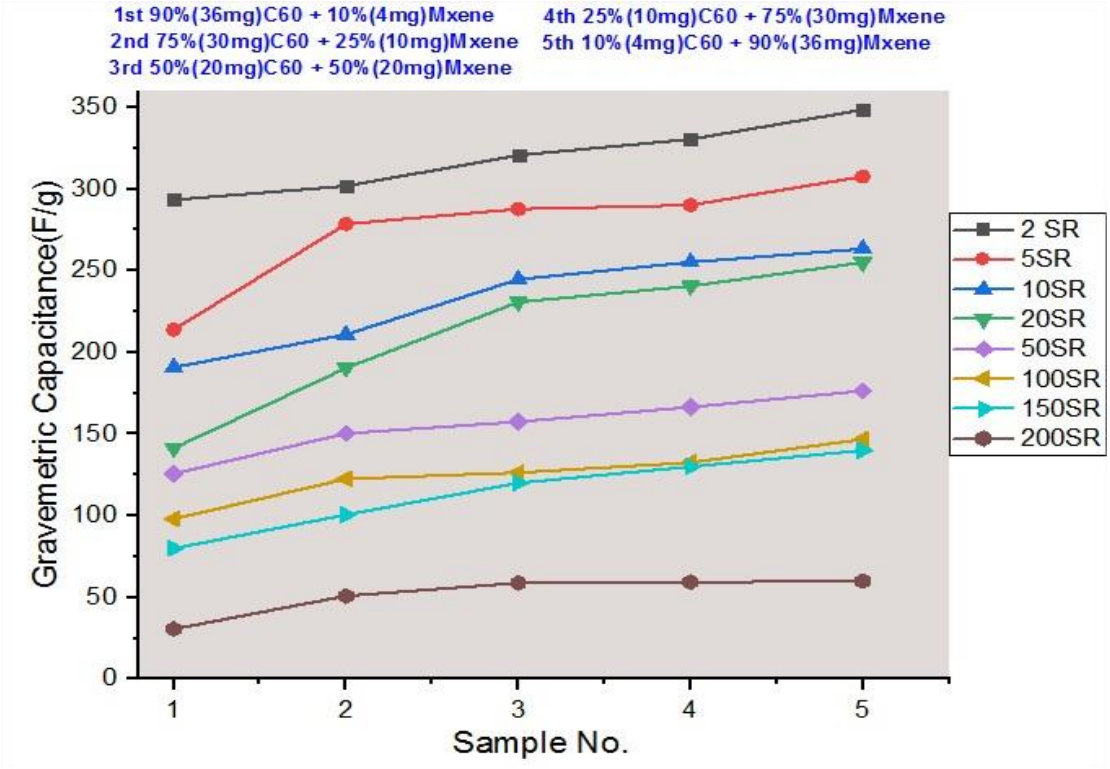

Figure 4-19: Capacitance of all samples at different scan rates

Chapter 05

5. CONCLUSION AND FUTURE RECOMMENDATIONS

5.1 Conclusion

MXene + C60 nanocomposite were successfully made suing dispersion of MXene in DI and Dispersion C60 in Ethanol. Phase purity with good crystalline Structure obtained and verified through XRD results. Capacitance of Novel material increased successfully as compared to pure MXene. Capacitance for pure MXene (200-250 F/g) at 2 Scan rate is increased with mixture of C60 to 348F/g at 2 scan rate. In this research we increase 29% capacitance of MXene with mixture of C60 (Fullerene). Novel composite exhibited dense, uniform surface morphology which is verified through SEM analysis. Nanocomposite of MXene and C60 shows higher mobility and low resistivity due to compact and large grain size with minimum grain boundaries for electrical properties. Capacitance with C60 only have value around 150 Fg^{-1} but with mixture of MXene capacitance increased to some extends. After finding capacitance of all samples at different scan rates we came to know that the major effect in increase of capacitance is due to MXene not due to C60.

5.2 Future Recommendations

From all obtained results and observation, the conclusion provides the outcomes of thesis along with some important future recommendations in fabrication of electrodes for super capacitors using materials C60 and MXene. Some of important future recommendations are listed below:

- Capacitance of MXene/C60 base supercapacitor can be optimized by decreasing the concentration of C60.
- By using some other 0D materials with MXene may be used to optimize and enhance the capacitance of a super capacitors along with fabrication of electrodes.
- Other composites of MXene with other 0D, 1D and 2D materials can be proposed in order to improve specific capacitance of supercapacitor.

6. REFERENCES

[1] Conway, B.E (1999). “Electrochemical Super capacitors: Scientific Fundamentals and Technological Applications”, 347: pp. 36-40.

[2] Burke, A. (2000). “Ultra-capacitors: why, how, and where is the technology.” *Journal of Power Sources,* 91(1): pp. 37-50

[3] Kotz R. and M. Carlen (2000). “Principle of applications o electrochemical capacitors.” *Electrochimica Acta,* 45(15-16): pp. 2483-2498.

[4] Qu, D. Y. and H. Shi (1998). “Studies of activated carbon used in doubke –layer capacitors,” *Journal of Power Sources,* 74(1): pp. 99-107.

[5] Zheng, J. P. and T. R. jow (1995). “A New Charge Storage Mechanism for Electrochemical Capacitors.” *Journal of the Electrochemical Society,* 142 (1): L6-L8.

[6] Shi, H. (1996). “Activated carbon and double layer capacitance.” *Electochimica Acta* 41(10): pp. 1633-1629.

[7] Kin, I. H., J. H. Kim, et al. (2005). “Electrochemical characterization of electrochemically prepared ruthenium oxide/carbon nanotubes electrode for super capacitors applications.” *Electrochemical and solid-state letters,* 8(7): pp. A369-A371.

[8] Frachowiak, E., K. Metenier, el al. (2000). “Super capacitor electrode from multiwalled carbon nanotubes.” *Applied physics Letters,* 77(15): pp. 2421-2423.

[9] Conway, B. E., V. Birss, el al. (1997). “The role and utilization of pseudo capacitance for energy storage by super capacitor.” *Journal of Power Sources,* 66(1-2): pp. 1-14.

[10] Ryu, K. S., K. M. Kin, et al. (2002). “Symmetric redox super capacitor with conducting polyaniline electrodes.” *Journal of Power Sources,* 103(2): pp. 305-309.

[11] Arbizzani, C., M. Mastragostino, et al. (2001). “New trends in electrochemical super capacitors.” *Journal of power sources,* 100(1-2): pp. 164-170.

[12] An, K. H., K. K. Jeon, at al. (2002). "High-capacitance super capacitor using Nano composite electrode of single-walled carbon nanotubes and polypyrrole." *Journal of electrochemical Society*, 149(8): pp. A1058-A1062.

[13] Zheng, J. P., P. J. Cygan, et al. (1995). "Hydrous Ruthenium Oxides as an electrode material for Electrochemical Capacitors." *Journal of the electrochemical Society*, 142(8): pp. 2699-2703.

[14] Jurewics, K., S. Delpeux, at al. (2001). "Super capacitor from nanotubes/polypyrrole composites." *Chemical Physics Letters*, 347(1-3): pp. 36-40.

[15] Repp, Sergej, Harputlu, Ersan, Gurgen, Seda . "Synergetic Effects of Fe3+ doped Spinel Li4Ti5O12 Nanoparticles on Reduced Graphene Oxide for High Surface Electrode Hybrid Supercapacitors." *Nanoscale* (10): pp. 1039 – 1040.

[16] M. Naguib et al., "Two-dimensional Nano crystals produced by exfoliation of Ti_3AlC_2." *Advance Matter*. 23 (37): (2011), pp. 4248–4253.

[20] M. Naguib et al., "New two-dimensional niobium and vanadium carbides as promising materials for li-ion batteries." *J. Am. Chem. Soc*, 135 (43): (2013), pp. 15966–15969.

[21] M. Naguib et al., New two-dimensional niobium and vanadium carbides as promising materials for li-ion batteries, J. Am. Chem. Soc. 135 (43): (2013), pp. 15966–15969.

[22] M. Ghidiu et al., "Synthesis and characterization of two-dimensional Nb_4C_3(MXene)." C*hem. Commun.* 50 (67): (2014), pp. 9517–9520

[23] M. Naguib et al., "Two-dimensional transition metal carbides." *ACS Nano* 6 (2): (2012), pp. 1322 - 1331.

[24] M. Ghidiu, M.R. Lukatskaya, M.Q. Zhao, Y. Gogotsi, M.W. Barsoum, "Conductive 2-Dimensional titanium carbide 'clay' with high volumetric capacitance." *Nature*, 516 (7529): (2015), pp. 78–81.

[25] A. Djire, A. Bos, J. Liu, H. Zhang, E.M. Miller, N.R. Neale, "Pseudo capacitive storage in Nano layered Ti2NTx MXene using Mg-ion electrolyte." *ACS Appl. Nano Mater*. 2 (5): (2019), pp. 2785–2795.

[26] B. Anasori et al., “Two-dimensional, ordered, double transition metals carbides (MXenes).” *ACS Nano*, 9 (10): (2015), pp. 9507–9516.

[27] X. Wu, Z. Wang, M. Yu, L. Xiu, J. Qiu, “Stabilizing the MXenes by carbon Nano plating for developing hierarchical Nano hybrids with efficient lithium storage and hydrogen evolution capability.” *Adv. Mater,* 29 (24): (2017) pp. 1–8.

[28] E. Pomerantseva, Y. Gogotsi, “Two-dimensional heterostructures for energy storage.” *Nat. Energy,* 2 (7): (Jul. 2017) pp. 1–6.

[29] Stoller M D,Park S J, Zhu Y W, An J H and Ruoff R S. (2008) *NanoLet,*. (8): pp. 3498–502.

[30] Lei Z, Lu L and Zhao X S. (2012), *Energy Environ. Sci.* (5): pp. 6391–6399.

[31] X. Li, H. Zhu, “Two-dimensional MoS2: properties, preparation, and applications.” *J. Materiom.* 1 (1): (2015), pp. 33–44.

[32] H. Zhang, “Ultrathin two-dimensional nanomaterials.” *ACS Nano,* 9 (10): (2015), pp. 9451–9469.

[33] M.Y. Li, C.H. Chen, Y. Shi, L.J. Li, “Heterostructures based on two-dimensional layered materials and their potential applications.” *Mater. Today* 19 (6): (2016), pp. 322–335.

[34] X. Huang, Z. Zeng, H. Zhang, “Metal dichalcogenide nanosheets: preparation, properties and applications.” *Chem. Soc. Rev.* 42 (5): (2013), pp. 1934–1946.

[35] S. Das, M. Kim, J.W. Lee, W. Choi, “Synthesis, properties, and applications of 2- D materials: a comprehensive review.” *Crit. Rev. Solid State Mater. Sci.* 39 (4): (2014), pp. 231–252.

[36] X. Huang, Z. Zeng, H. Zhang, “Metal dichalcogenide nanosheets: preparation, properties and applications.” *Chem. Soc. Rev.* 42 (5): (2013), pp. 1934–1946.

[37] J. Feng et al., “Metallic few-layered VS2 ultrathin nanosheets: high two-dimensional conductivity for in-plane supercapacitors.” *J. Am. Chem. Soc.* 133 (44): (2011), pp. 17832–17838.

[38] P.S. Toth et al., “Asymmetric MoS2/graphene/metal sandwiches: preparation, characterization, and application.” *Adv. Mater.* 28 (37): (2016), pp. 8256–8264.

[39] X. Liu, I. Balla, H. Bergeron, G.P. Campbell, M.J. Bedzyk, M.C. Hersam, "Rotationally commensurate growth of MoS2 on epitaxial graphene." *ACS Nano* 10 (1): (2016): pp. 1067–1075.

[40] L. Jiang et al., "Monolayer MoS2-graphene hybrid aerogels with controllable porosity for lithium-ion batteries with high reversible capacity." *ACS Appl.* Mater. Interfaces 8 (4): (2016), pp. 2680–2687.

[41] Y. Zheng et al., "Recent advances of two-dimensional transition metal nitrides for energy storage and conversion applications." *Flat Chem* (19): (2020), pp. 100149.

[42] Y.G. Wang, H.Q. Li, Y.Y. Xia, "Ordered whisker like polyaniline grown on the surface of mesoporous carbon and its electrochemical capacitance performance." *Adv. Mater*. 18, (2006), pp. 2619–2623.

[43] C.C. Hu, K.H. Chang, M.C. Lin, Y.T. Wu, "Design and tailoring of the nanotubular arrayed architecture of hydrous RuO2 for next generation supercapacitors." *Nano Lett.* 6, (2006), pp. 2690–2695

[44] I. Sapurina, M. Mokeev, V. Lavrentev, V. Zgonnik, M. Trchová, D. Hlavatá, J. Stejskal, Polyaniline complex with fullerene C60, Eur. Polym. J. 36 (2000) 2321– 2326.

[45] H. Li, J. Wang, Q. Chu, Z. Wang, F. Zhang, S. Wang, "Theoretical and experimental specific capacitance of polyaniline in sulfuric acid." *J. Power Sources* 190, (2009), pp. 578–586.

[46] Y. Wei, J. Tian, A.G. MacDiarmid, J.G. Masters, A.L. Smith, D. Li, "Preparation and conductivities of fullerene-doped polyanilines." *J. Chem. Soc. Chem. Commun. 7*, (1993), pp. 603–604.

[47] S. Xiong, F. Yang, H. Jiang, J. Ma, X. Lu, "Covalently bonded polyaniline/fullerene hybrids with coral-like morphology for high-performance supercapacitor." *Electrochim. Acta 85*, (2012), pp. 235–242.

[48] C. Park, E. Yoon, M. Kawano, T. Joo, H.C. Choi, "Self-crystallization of C70 cubes and remarkable enhancement of photoluminescence." *Angew. Chem. Int. Ed*, 49, (2010), pp. 9670-9675.

[49] P.D. Hale, Discrete-variational-X.alpha. "Electronic structure studies of the spherical C60 cluster: prediction of ionization potential and electronic transition energy" *J. Am. Chem. Soc.* 108, (1986), pp. 6087e6088.

[50] T. Wakahara, P. D'Angelo, K.i. Miyazawa, Y. Nemoto, O. Ito, N. Tanigaki, D.D.C. Bradley, T.D. Anthopoulos, "Fullerene/cobalt porphyrin hybrid nanosheets with ambipolar charge transporting characteristics." *J. Am. Chem. Soc. 134,* (2012). pp. 7204-7206.

[51] T. Kodama, M. Ohnishi, W. Park, T. Shiga, J. Park, T. Shimada, H. Shinohara, J. Shiomi, K.E. Goodson, "Modulation of thermal and thermoelectric transport in individual carbon nanotubes by fullerene encapsulation." *Nat. Mater. 16,* (2017), pp. 892.

[52] K. Minami, Y. Kasuya, T. Yamazaki, Q. Ji, W. Nakanishi, J.P. Hill, H. Sakai, K. Ariga, "Highly ordered 1D fullerene crystals for concurrent control of macroscopic cellular orientation and differentiation toward large-scale tissue engineering" *Adv. Mater. 27,* (2015), pp/ 4020-4026.

[53] T. Kodama, M. Ohnishi, W. Park, T. Shiga, J. Park, T. Shimada, H. Shinohara, J. Shiomi, K.E. Goodson, "Modulation of thermal and thermoelectric transport in individual carbon nanotubes by fullerene encapsulation." *Nat. Mater. 16*, (2017), pp. 892.

[54] Q.-Z. Zhang, D. Zhang, Z.-C. Miao, X.-L. Zhang, S.-L. Chou, "Research progress in MnO2 -carbon based supercapacitor electrode materials." *Small 14*, (24): (2018), pp. 1702883.

[55] Z. Yu, L. Tetard, L. Zhai, J. Thomas, "Supercapacitor electrode materials: nanostructures from 0 to 3 dimensions." *Energy Environ. Sci. 8 (3):* (2015), pp. 702–730.

[56] H. Jiang, P.S. Lee, C. Li, "3D carbon-based nanostructures for advanced supercapacitors." *Energy Environ. Sci. 6 (1)*: (2013), pp. 41–53.

[57] P. Salles, E. Quain, N. Kurra, A. Sarycheva, Y. Gogotsi, "Automated scalpel patterning of solution processed thin films for fabrication of transparent MXene microsupercapacitors." *Small*, (2018), pp. 1802864.

[58] L. Li, R. Li, S. Gai, P. Gao, F. He, M. Zhang, et al., "Hierarchical porous CNTs@NCS@ MnO2 composites: rational design and high asymmetric supercapacitor performance." *J. Mater. Chem. 3 (30)*: (2015), pp. 15642–15649.

[59] H.R. Naderi, P. Norouzi, M.R. Ganjali, "Electrochemical study of a novel high-performance supercapacitor based on MnO 2/nitrogen-doped graphene nanocomposite." *Appl. Surf. Sci. 366*, (2016), pp. 552–560.

[60] J. Zhu, youlong Xu, J. Hu, L. Wei, J. Liu, M. Zheng, "Facile synthesis of MnO 2 grown on nitrogen-doped carbon nanotubes for asymmetric supercapacitors with enhanced electrochemical performance." *J. Power Sources 393*, (2018), pp. 135–144.

[61] X. Ou, Q. Li, D. Xu, J. Guo, F. Yan, "Insitu growth of MnO2 nanosheets on N-doped carbon nanotubes derived from polypyrrole tubes for supercapacitors." *Chem. Asian J. 13 (5):* (2018), pp. 545–551.

[62] Y. Wen, T.E. Rufford, X. Chen, N. Li, M. Lyu, L. Dai, L. Wang, "Nitrogen-doped Ti 3 C 2 T x MXene electrodes for high-performance supercapacitors." *Nanomater. Energy 38*, (2017), pp. 368–376.

[63] Zhang Y, Lin B, Sun Y, Han P, Wang J, Ding X, Zhang X, Yang H. "MoO2@Cu@C composites prepared by using polyoxometalates@ metal-organic frameworks as template for all-solid-state flexible supercapacitor." *Electrochim Acta 188:* 2016; pp. 4-8.

[64] Cui C, Wei Q, Zhou L, Mai L, Ma J. "Facile synthesis of MoO2@ C nanoflowers as anode materials for sodium-ion batteries." *Mater Res Bull* 94: 2017, pp. 122-126.

[65] Si H, Sun L, Zhang Y, Zhang Y, Bai L, Zhang Y. "Carbon-coated MoO2 nanoclusters anchored on RGO sheets as high-performance electrodes for symmetric supercapacitors." *Dalton Trans 48:* 2019, pp. 285-295.

[66] S. H. Yun, and J. Z. Wu, Appl. *Phys. Lett.68*, (1996), pp. 862.

[67] M. Annabi, A. M. Chirgui, F. B. Azzuoz, and M. B. Salem, *Physica C 25*, (2004), pp. 405.

[68] K. Semba, A. Matsuda, and T. Ishii, *Phys. Rev*. B 49, (1996), 10043.

[69] M. K. Wu, J. R. Ashburn, C. J. Torng, P. H. Hor, R. L. Meng, L. Gao, Z. J. Huang,Y. Q. Wang, and C.W. Chu, *Phys. Rev. Lett*. 58, (1987), pp. 908.

Completion Certificate

It is to certify that the thesis titled *"*Analysis of C60 and MXene Nanocomposite Based Electrode Materials for Energy Storage Devices*"* submitted by NS HASSAN BUKHARI, Registration No 00000275970 of MS Entry-2018 Electrical Engineering has been found satisfactory for requirement of degree of Masters of Science

Thesis Supervisor: _____

DR. SAIFULLAH AWAN